

CZECH TECHNICAL UNIVERSITY IN
PRAGUE

Faculty of Nuclear Sciences and Physical
Engineering

Department of Physics



Research project

Properties of the strong coupling
constant α_s in proton-proton
collisions

Bc. Lukáš Marek

Supervisor: Ing. Zdeněk Hubáček, Ph.D.

Prague, 2018

Declaration:

I declare that I wrote my research project independently and with help of the cited bibliography.

I agree with usage of this project in the purport of the Act 121/2000 (Copyright Act).

Prohlášení:

Prohlašuji, že jsem svůj výzkumný úkol vypracoval samostatně a použil jsem pouze podklady (literaturu, software, atd.) uvedené v příloženém seznamu.

Nemám závažný důvod proti užití tohoto školního díla ve smyslu 60 Zákona .121/2000 Sb., o právu autorském, o právech souvisejících s právem autorským a o změně některých zákonů (autorský zákon).

Název práce:

Zkoumání vlastností silné vazbové konstanty α_S v proton-protonových srážkách

Autor: Lukáš Marek

Obor: Experimentální jaderná a částicová fyzika

Druh práce: Výzkumný úkol

Vedoucí práce: Ing. Zdeněk Hubáček, Ph.D. Katedra fyziky, Fakulta jaderná fyzikálně inženýrská, České vysoké učení technické v Praze

Konzultant: _____

Abstrakt: Tento výzkumný úkol pojednává o silné vazbové konstantě α_S a jejích vlastnostech v proton-protonových srážkách. Hlavním přínosem práce je příprava na nadcházející diplomovou práci a to především v těchto bodech: seznámení se s tématem týkající se silné vazbové konstanty α_S , částečné shrnutí dosavadních výsledků, vygenerování vzorku dat pro teoretickou předpověď v monte carlo generátoru Pythia a nalezení vhodné proměnné pro vazbovou konstantu α_S , která by maximálně redukovala jak chybu teoretickou tak chybu experimentální. Vzorek dat je vygenerován při energii $\sqrt{s} = 13$ TeV se zvoleným rozhraním, které opovídá detektoru ATLAS (tune A14) a níže uvedenou volbou PDF sad pro několik různých hodnot α_S . Následně bylo provedeno zpracování anti- k_t jetovým algoritmem. Z výše uvedených důvodů byla vybrána dvoujetová azimutální korelace jako ideální pozorovatelná. V rámci této práce je ukázána její citlivost na několika jetové procesy, čemuž odpovídá úměrnost vazbové konstantně a zároveň velké snížení teoretických chyb.

Klíčová slova: QCD, silná vazbová konstanta α_S , jety a jetové algoritmy, dijetové azimutální korelace

Title:

Properties of the strong coupling constant α_S in proton-proton collisions

Author: Lukáš Marek

Abstract: This research project deals with the strong running coupling α_S and its properties in proton-proton collisions. Main benefit of this work is a preparation for the following diploma thesis and the contribution is primarily in next points: to become acquainted with the topic of the strong running coupling α_S , to partly summarise the contemporary results for the value α_S , to generate the data sample for the theoretical prediction in the Monte Carlo generator Pythia and to find a proper variable which would maximally reduce the theoretical and experimental uncertainties. The data sample was generated for several values of α_S with the central mass energy $\sqrt{s} = 13$ TeV within interface reflecting the ATLAS detector settings (tune A14) and with further mentioned PDF sets. Then, the anti- k_t jet algorithm processed the particle level data. Due to the previously discussed reasons, the dijet azimuthal correlation was chosen as the suitable observable. In the frame of this work, its sensibility for multijet events was demonstrated which have direct connection to α_S proportion and at the same time also the reduction of the theoretical uncertainties was shown.

Keywords: QCD, strong coupling constant α_S , jets and jet algorithm, dijet azimuthal correlation

Acknowledgement

I would like to express gratitude to my supervisor Zdeněk Hubáček for his patience, willingness and understanding and also to my college Vladimír Žitka and his supervisor Miroslav Myška for very helpful discussions about the research topic.

Contents

1	Introduction to Particle Physics	12
2	Theoretical concept of QCD	18
3	Experimental Framework	30
3.1	LHC and ATLAS detector	30
3.2	Physics of Jets	32
3.3	Jet algorithm	36
4	Monte Carlo prediction of α_S	40
4.1	Contemporary results for α_S from hadronic final state	40
4.2	Method for α_S prediction	42
4.3	Monte Carlo Generator Pythia	44
4.3.1	Tune and PDF selection	44
4.3.2	Theoretical Uncertainty	45
4.4	Data processing and selection of variables	46
4.4.1	Dijet Azimuthal Correlation	53
4.4.2	Ratio $R_{\Delta\phi}$	54
4.5	Expected continuation	58
5	Summary and Conclusion	59
	Literature	60

List of Figures

1	The summary of some experimental measurements of the strong coupling constant.[1]	11
1.1	The diagram of the Standard Model. [2]	13
1.2	The baryons octet of the $SU(3)$ group. [3]	16
2.1	The Feynman diagrams of the elemental vertices of QCD.	19
2.2	The Feynman diagram of the scattering of quark-quark. [4]	21
2.3	The Feynman diagrams of the scattering of quark-quark with the gluon (b) loop and fermion loop (a).[4]	22
2.4	The Feynman diagram of a propagation of a electron with the loops (a), the polarization effect of a medium with electric charge (b).[5]	23
2.5	The antiscreening effect of QCD with the Feynman diagram of this process. [5]	24
2.6	The graph of the strong coupling constant α_S as a function of the energy scale Q . [6]	25
2.7	The graph of PDF (multiplied by the Bjorken scale x) from the parametrisation MSTW 2008 in the NLO as a function of the Bjorken scale x . [7]	29
3.1	The scheme of the detector ATLAS.[8].	32
3.2	The scheme of the hard scattering of two partons with different stages of the process.[9]	34
3.3	The schematic depiction of infrared sensitivity and collinear of the jet algorithm.[10]	37
3.4	The graph of parton level events after usage of anti k_t algorithm.[11]	39

4.1	The measurement of the α_S with the usage of the colliders: HERA/PERTA, LEP and LHC (CMS). [12]	41
4.2	The measurement of the α_S with the usage of the detector CMS at LHC. [13]	42
4.3	The measurement of the α_S with the usage of the detector ATLAS at LHC and also a collection of results from other detectors (and accelerators) is involved. [14]	43
4.4	The boost effect and the definitions of y_{boost} and y^* . [15] . . .	48
4.5	The differential inclusive cross section $\frac{d\sigma}{dp_T}$ with the ratio graph.	50
4.6	The differential dijet cross section $\frac{d\sigma}{dm_{jj}}$ with the ratio graph. .	50
4.7	The normalized differential inclusive cross section $\frac{1}{\sigma} \frac{d\sigma}{d\Phi}$ with the ratio graph.	51
4.8	The normalized differential inclusive cross section $\frac{1}{\sigma} \frac{d\sigma}{dy}$ with the ratio graph.	51
4.9	The double differential inclusive cross section $\frac{d\sigma}{dp_T y}$	52
4.10	The double differential inclusive cross section $\frac{d^2\sigma}{dp_T y}$. [16]	52
4.11	The scheme of the azimuthal angle $\Delta\Phi_{dijet}$ for the dijet system with a different number of additional partons. [15].	53
4.12	The dijet azimuthal correlation by the ATLAS (left) and CMS (right) detector in the p_T intervals [17, 18]	54
4.13	The differential cross section $\frac{1}{\sigma} \frac{d\sigma}{d\Delta\Phi}$ with the ratio plot.	55
4.14	The ratio of data and theoretical prediction with the PDF and scale uncertainties.[18]	55
4.15	The ratio quantity $R_{\Delta\Phi}$ for the different intervals of variables y^* and $\Delta\Phi_{max}$. [14]	57
4.16	The ratio quantity $R_{\Delta\Phi}$ for the different intervals of variables y^* and $\Delta\Phi_{max}$	57

Introduction

The main purpose of Particle Physics is to study basic constituents of matter and their mutual interaction. Nowadays, the high energy collisions of hadrons are one of the most exploited way to achieve this purpose. In this context, the next natural step is an attempt to describe the experimental data with a theoretical concept and, according to this theory, make a prediction for another measurement/observation.

Currently, the most successful theoretical description is offered by the Standard Model, where one of its elementary parameters is the strong coupling constant α_S which is an indispensable part of the theory describing strong interaction, the quantum chromodynamics (QCD). The strong coupling enters all calculations of the strong interaction either as an explicit part of the matrix elements or as an implicit part of the evolution equations for parton distribution functions. It is the only one free parameter (besides quarks masses) which has to be inserted into QCD.

Therefore a great effort has been made to perform the most precise measurement of this running constant. A very illustrative example of the importance of the precise α_S measurement is the Higgs cross section presented in [1]. One of the possible ways for the determination of the $\alpha_S(m_Z^2)$ value are the lattice QCD with the result: $\alpha(m_Z^2) = 0.11840 \pm 0.00060$ and a jet shape variable, thrust, for the positron-electron scattering with the outcome: $\alpha(m_Z^2) = 0.1135 \pm 0.00105$. This difference of prediction α_S causes a large change of the Higgs boson cross section of is about 8%–9%. This is much more than any theoretical or experimental uncertainty. It can be shown that only less than 1% of uncertainty of α_S is tolerable in the perspective of the Large Hadron Collider (LHC) measurements.

Some of the existing results can be seen in Figure 1 where ways to measure the α_S with their uncertainties are shown. The most utilized observables and processes for extracting the value are [19]:

- Deep inelastic scattering
- Hadronic Z-decays
- Event shapes and jets in electron-positron annihilation
- Jets in hadron-hadron collisions
- Hadronic τ -decays
- Heavy quarkonia decay
- Lattice QCD

For this project, jets in hadron-hadron collisions were chosen with the focus on the proton-proton hard scattering at the LHC detected with ATLAS detector. The primary goal is to make a preparation for the following diploma thesis. Due to this reason the discussion is done in a mostly theoretical qualitative way with some results in the last part of this research paper.

The first chapter of this thesis discusses the Particle Physics and the Standard Model with a further focus on the history of QCD. The second chapter offers elementary information about quantum chromodynamics and its basic properties: a formulation of QCD with Lagrange formalism, the running nature of the parameter α_S in context of the renormalization procedure, the color confinement and the asymptotic freedom. The second part of this chapter also includes basic principles of the quark-parton model and of the parton distribution functions. The third chapter discusses basic variables needed for the hard scattering characterisation, also brief introduction to jet physics and the description of ATLAS detector. The fourth chapter concerns with the theoretical prediction for the parameter α_S . Its main goal is to determine the most suitable observable in accordance with mentioned requirements with the final results summarised in the fifth chapter.

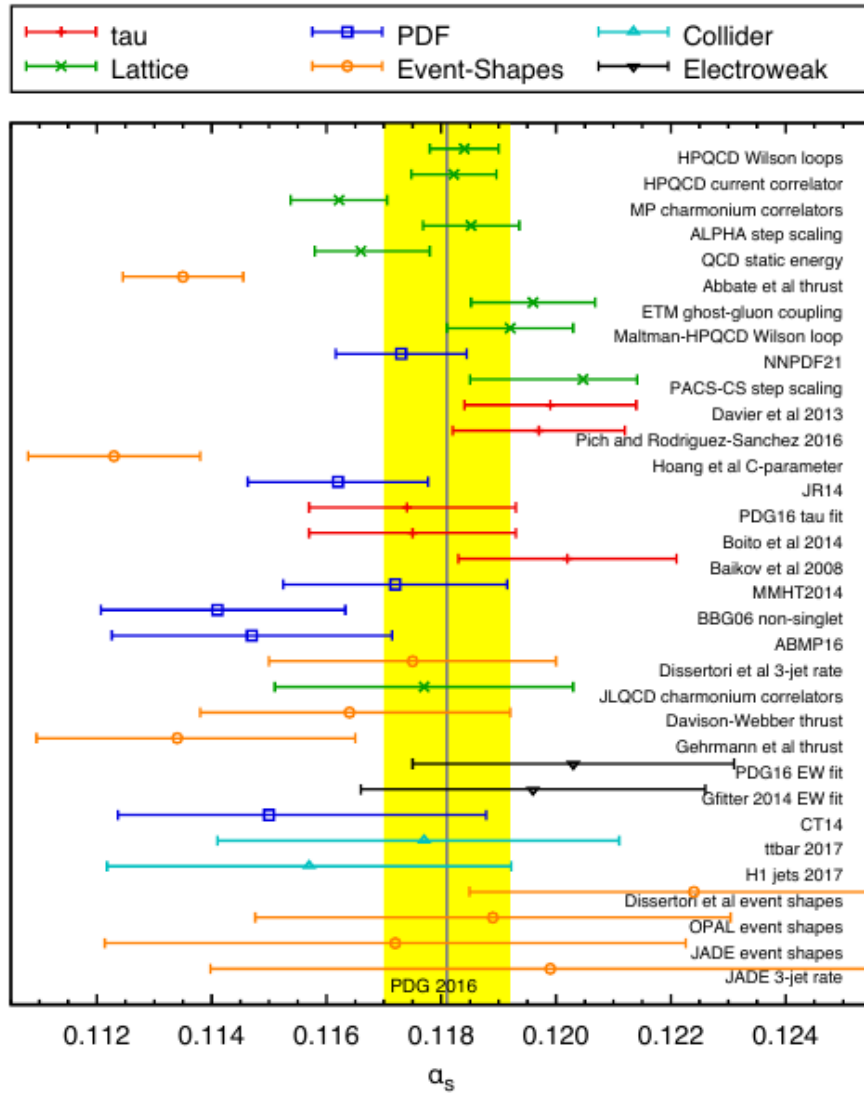


Figure 1: The summary of some experimental measurements of the strong coupling constant.[1]

Chapter 1

Introduction to Particle Physics

One of the cornerstones of Particle Physics is the Standard Model (SM). It is a theoretical concept which attempts to describe three interactions of nature acting between elementary particles, based on current experimental results. These three interactions include: the **weak interaction**, the **electro-magnetic interaction** and the **strong interaction**. The gravitational interaction, which is much more common to everyday observation, is not successfully comprised in the SM. Also, it may be neglected due to its very low relative strength in comparison with the other elementary forces for achieved energies in contemporary accelerators (see further in Table 1.1).

Elementary particles can be divided into two categories according to the value their of spin: **fermions** with half-integer spin and **bosons** with integer spin¹ (see Figure 1.1).

Fermions can be further divided into two families of **leptons** and **quarks**². The electron e^- is the most common lepton (with the negative electric charge). It was discovered by J. J.Thomson in 1897 during an investigation of the cathode rays.[20] In the perspective of quarks, there can be no direct examination of their existence due to the properties of the strong interaction called color or quark confinement (it is explained further in the text), which restricts the observation only to bound states of quarks, baryons and

¹This different value has a consequence in distinct behaviour in the sense the of Pauli exclusion principle. Fermions must obey the principle and therefore there is zero probability that two fermions could be observed in the same quantum state. Bosons, on the contrary, are not restricted to this principle and any number of bosons could occupy the same quantum state.

²Further, they can be distinguished into three generations. See Figure 1.1.

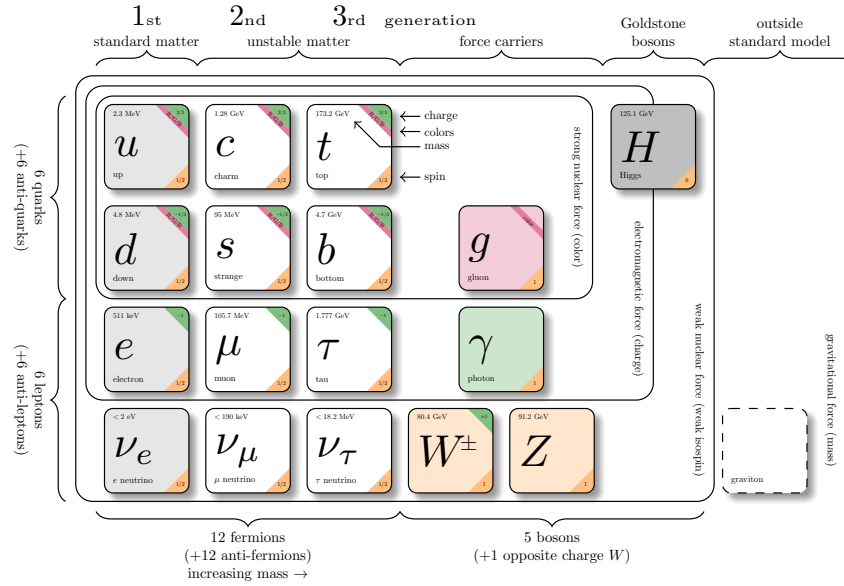


Figure 1.1: The diagram of the Standard Model. [2]

mesons³. The most familiar representatives of hadrons are proton and neutron (nucleons). The proton was first confirmed experimentally by E. Rutherford in 1911 [21]. At the time of discovery of proton and electron, it was quiet natural to regard them as elementary and therefore they were used as constituents of the first atomic models (the Rutherford model of atom). Similar situation has happened with leptons, quarks and bosons in the case of the SM, and because there is still no evidence of the internal structure, they are denoted and used as elementary particles. Leptons and quarks also have second and third generation which is mostly compound of unstable particle and therefore they are not basic constituents of matter.

As was mentioned before, the second category of elementary particles are bosons, which play a crucial role in the SM and in characterization of the interaction. Their important goal in the framework of the SM is to mediate the interactions. More precisely, in the case of scattering of two particles with electric charges, is in the lowest approximation described as

³Baryons are composed of three quarks and mesons are composed of one quark and one antiquark.

Interaction	Boson	M [GeV/c ²]	F_R [-]	r [fm]
Electro-magnetic	γ (photon)	0	10^{-2}	∞
Weak	W^\pm, Z (intermediate bosons)	80.4 and 91.2	10^{-6}	10^{-18}
Strong	$g_i, i = 1, \dots, 8$ (gluons)	0	1	$< 10^{-15}$
Gravitational	G (graviton)	0	10^{-8}	∞

Table 1.1: The description of the basic properties of the elementary interactions where F_R represents the relative strength and r stands for the range of the given force.[6])

an exchange of a photon with an amount of momentum between these two particles. Each interaction is then represented/mediated by different gauge bosons: one massless photon for the electromagnetic, heavy Z and W^\pm bosons for the weak and eight massless gluons for the strong interaction. The last piece of puzzle of the SM is the Higgs boson and the Higgs mechanism. This principle is accounted for generation of masses of all particles. Specifically, in first step the masses of Z and W^\pm are created by introducing the mechanism and the Higgs boson itself is established. In second step, the masses of all other particles are caused by an interaction with the Higgs field (with the Higgs boson).

From a mathematical and physical point of view, the SM is a local gauge quantum field theory based on product $SU(3) \times SU(2) \times U(1)$ gauge groups. The $SU(3)$ group represents the quantum chromodynamics, that describes the strong interaction between colored objects (gluons and quarks), the $SU(2)$ group corresponds with the weak interaction, that acts between fermions and leptons (they can be characterized by weak isospin I_3), and the $U(1)$ group stands for the electro-magnetic interaction between particles with the hyper-charge Y ⁴.

The SM is only an attempt to understand the present experimental observations. On one hand, there are many physical processes which were

⁴Hyper-charge Y and weak isospin I_3 can be related to electric charge Q as follows: $Q = I_3 + Y$.

theoretically understood and described with the SM, but on the other hand, even now lots of evidences of the SM incompleteness are known. As was previously mentioned, the gravitational interaction is one of the missing pieces in the SM. A question about larger portion of matter than anti-matter is still open⁵. Lots of new theories are already present that strive to explain all these problems (Supersymmetry (SUSY), Grand Unified Theories).

This brief section focuses on first steps towards QCD. The Eightfold Way theory by M. Gell-Mann [22] tries to explain properties of hadrons in sense of a group flavour symmetry $SU(3)$, then the discovery of quark structure of hadrons in the SLAC continued by the improvement of the quark theory called quark-parton model by R. Feynman and in the end, the color charge, that is the quantum characteristic of the particles interacting with the strong force, and its experimental confirmation are discussed.

In the middle of the 20th century many discoveries of new particles happened, mainly of hadrons (firstly, cosmic rays were used and further, with development of accelerator physics and technology, a high energy accelerator beams of leptons and hadrons were utilized). With these new "zoo" of particles the need for some theory framework which would categorize them in some way emerged. The first pioneers in this field were M. Gell-Mann and Y. Ne'eman. Both of them, independently, invented a theory which is able to interpret the new particles with the help of a symmetry group $SU(3)$ (as its representation). They had noticed that some quantum numbers of the hadrons (third component of isospin I_3 , hypercharge Y , electric charge Q , strangeness S , baryon number B) perform symmetries within the strong interactions and one of the consequences is the conservation of an electric charge Q and its relation with Y and I_3 is called Gell-Mann-Nishijima formula [23]:

$$Q = I_3 + \frac{Y}{2}. \quad (1.1)$$

Gell-Mann and Nishijima also established the relation between Y , S and B : $Y = S + B$ ⁶. One of the biggest successes of this theory was the prediction of the new hadron Ω^- which had not been yet observed. The prediction introduced not only the existence itself but also its mass, life-time and a way of production. In the year 1964 [24], this new hadron was detected at the

⁵The SM predicts that both of them should have been created in the same amount.

⁶Later, more quantum numbers was discovered with new hadrons and added to this equation.

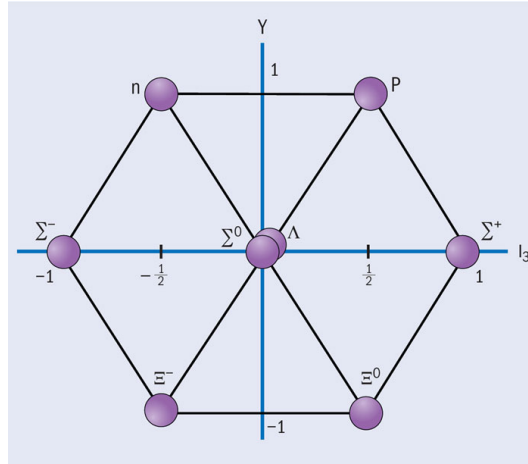


Figure 1.2: The baryons octet of the $SU(3)$ group. [3]

Brookhaven National Laboratory. One of the geometrical representation of the group $SU(3)$ can be seen in Figure 1.2.

Nevertheless, the theory also anticipated the basic triplet of the $SU(3)$ group comprehending "peculiar" particles with a non-integer spin and electric charge which were never observed in nature. M. Gell-Mann [25] and G. Zweig (in 1964) offered a theoretical solution of this ambiguity and proposed the quark model in which the hadrons are objects composed of the basic triplet of the $SU(3)$ group, quarks.

In the beginning of 1970 in the SLAC experiments on the inelastic scattering of electrons and protons were performed, among others, with an attempt to probe the Gell-Mann and Zweig quark theory. The result for the cross section of the process indicated a very interesting feature which had been earlier described by J. Bjorken [26] called Bjorken scaling. The cross-section depends on two kinematic Lorentz invariant variables: the virtual photon mass and the energy transfer. In case of the scattering electrons on protons, the structure functions are also included in formula and depend on these variables. In high energy transfer, the Bjorken scaling causes that these structure functions depend only on their ratio. R. Feynman used these results as a basis for a new theory which is called the parton model. In the frame of this model, he interpreted the Bjorken scaling as a composite nature of proton consist of point-like components, partons⁷ [27].

⁷He did not denote partons only as quarks.

One of the consequences of the parton model is that the bound state of three quarks sss , baryon Ω^- , has a symmetric space part of wave function and all the quarks are in the same quantum state. This is clearly in contradiction with the Pauli exclusion principle and the antisymmetric space-function of Ω^- . The solution for this problem was establishing a new quantum number called color charge (H. Fritzsch and M. Gell-Mann in 1971[3]) which should be different for all the quarks in Ω^- and conserved in the frame of the strong interaction. The requirement for the three different types ($N_C = 3$) and its existence itself was proven from an experimental observation of the cross-section for the electron-positron annihilation into muons and hadrons. The observed variable was the ratio of the cross sections of these two different annihilations:

$$\frac{\sigma(ee^+ \rightarrow q\bar{q})}{\sigma(ee^+ \rightarrow \mu\mu^+)} = \sum_q \left(\frac{Q_q}{e} \right)^2 N_C, \quad (1.2)$$

where Q_q represents electric charge of quark. Only the prediction with $N_C = 3$ was in agreement with the data.

Chapter 2

Theoretical concept of QCD

The goal of this chapter and the following sections is to present a basic description of QCD in the Lagrange formalism and its elementary properties among which the running of coupling α_S and the asymptotic freedom (associated with the color confinement) can be classified. Brief introduction to the theme of the perturbative QCD (pQCD) is also included.

In the beginning, an effort is made to clarify the expressions that determine QCD as a local nonabelian gauge quantum field theory (especially the words "local", "nonabelian" and "gauge"). The strong interaction acts between particles with color charges that is distinguished to three different types (labelled green (g), red (r), blue (b)). These particles can be described with a help of the Dirac bispinors $\psi(x)$:

$$\psi(x) = \begin{pmatrix} \psi_r(x) \\ \psi_g(x) \\ \psi_b(x) \end{pmatrix}. \quad (2.1)$$

It has to be symbolized as matrix in the color space due to these distinct types. According to the Dirac field theory its free Lagrangian and generated Euler-Lagrange equation have following form:

$$\begin{aligned} \mathcal{L}_{free}^{fermion} &= \bar{\psi}(x)(i\gamma^\mu\partial_\mu - m)\psi(x), \\ (i\gamma^\mu\partial_\mu - m)\psi(x) &= 0, \end{aligned} \quad (2.2)$$

where γ_μ represents the Dirac matrices and m mass of the particle. For QCD, the local gauge transformation is defined by:

$$\psi'(x) \equiv \exp[i\alpha_a(x)T_a]\psi(x) = U\psi(x), \quad a = 1, \dots, 8, \quad (2.3)$$

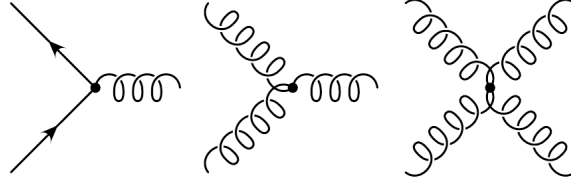


Figure 2.1: The Feynman diagrams of the elemental vertices of QCD.

where T_a are generators of the color $SU(3)$ group, which is created by these transformations, and $\alpha_a(x)$ are parameters of this transformation. The dependence of the parameters on space-time coordinate x is called local. It can be seen that the application of this transformation on the Dirac bispinor in the free Lagrangian (Equation 2) causes the noninvariance and can be eliminated by the introduction of a gauge field A_μ and the special derivate, called the covariant derivate:

$$D_\mu \equiv \partial_\mu - igA_\mu, \quad A_\mu = A_\mu^a T_a. \quad (2.4)$$

These fields are interpreted as 8 gauge field bosons of the strong force, gluons. The transformation of these fields A_μ is defined in following way:

$$A_\mu^{a'} = A_\mu^a + f_{bca} \alpha_b A_\mu^c + \frac{1}{g} \partial_\mu \alpha_a, \quad (2.5)$$

where f_{abc} represents the structure constants. Their important role in the whole formalism is to establish relation between the generators:

$$[T^a, T^b] = if_{abc} T^c. \quad (2.6)$$

This feature of the transformation is called nonabelian and has a great consequence for the behaviour of the strong interaction. For the implementation of the gauge field to QCD Lagrangian, the invariant tensor of A_μ is needed to derive with the final form:

$$F_a^{\mu\nu}(x) = \frac{\partial A_a^\nu(x)}{\partial x_\mu} - \frac{\partial A_a^\mu(x)}{\partial x_\nu} - gf_{abc} A_b^\nu(x) A_c^\mu(x). \quad (2.7)$$

As can be seen from the above equation, self interactions of the gauge field is present due to the nonabelian conduct of the generators and the theory itself. In case of the abelian QED, this member of the invariant tensor is

missing. Now, it is possible with all the information to construct the QCD Lagrangian:

$$\mathcal{L}^{QCD} = \bar{\psi}(x)(i\gamma^\mu\partial_\mu + m)\psi(x) + \alpha_S\bar{\psi}(x)\gamma^\mu\psi(x)T^a A_\mu^a(x) - \frac{1}{4}G^{\mu\nu a}(x)G_{\mu\nu}^a(x), \quad (2.8)$$

where α_S is the coupling constant of QCD and it will be discussed later. From QCD Lagrangian it is apparent that the first member stands for the free Lagrangian, the second member represents the interaction between the gauge field A_μ and the particle (between the gluon field and the fermion field, see Figure 2.1; the first diagram) and the last member is the potential term of the gauge field. The self interaction can be easily extracted from a detailed product of these two gauge tensors:

$$\begin{aligned} \mathcal{L}^{gauge} \cong & (\partial_\nu A_\mu^a - \partial_\mu A_\nu^a)(\partial^\nu A^{\mu a} - \partial^\mu A^{\nu a}) \\ & + g f_{abc}[(\partial_\nu A_\mu^a - \partial_\mu A_\nu^a)A^{\mu b}A^{\nu c} + (\partial^\nu A^{\mu a} - \partial^\mu A^{\nu a})A_\mu^b A_\nu^c] + g^2 f_{abc}f_{ade}A^{\mu b}A^{\nu c}A_\mu^d A_\nu^e, \end{aligned} \quad (2.9)$$

the presence of the four gauge field in one product is the self interaction of the four gluons and the same for the three gauge fields (see Figure 2.1; the second and the third diagram). This two interactions will help us to understand the principle of an antiscreening nature of the strong force.

Next section informs about the renormalization procedure for QCD and its effects on behaviour of the coupling α_S . In frame of the description of this consequence, the color confinement and asymptotic freedom (the antiscreening conduct) is described.

Following the QCD Lagrangian (Equation 2.8), a direct way should be to solve the Euler-Lagrange equations. During evaluation of these equations many mathematical problems appear which are hard to solve even with using of a computer capacity. Therefore, an approximate solution has to be used which is offered by the perturbative QCD (pQCD) or by the lattice QCD (lQCD, and by many other models). The goal of pQCD is to rewrite the explicit solution to the perturbative series in order of the coupling α_S which includes a free solution and a solution containing an interaction. This method was summarised by R. Feynman to so called Feynman rules. They are very easy and straightforward to use for a computation of many quantum variables of a process in QCD.

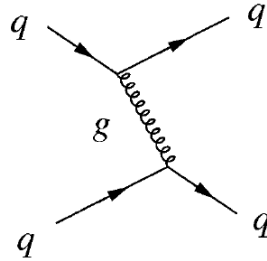


Figure 2.2: The Feynman diagram of the scattering of quark-quark. [4]

Previous statement is valid until the first order of pQCD (the leading order, LO), for example the scattering of two quarks which is depicted in Figure 2.2. With higher orders, more diagrams have to be counted in the invariant amplitude of the process and the complexity of the computation increases. The first problem is occurring with the loops (see Figure 2.3). One of the Feynman rules orders to integrate over momentum of all virtual particles in the loop within the full momentum-space (due to the Lorentz invariance, there is no natural cut-off). The result is a logarithmic UV divergence of the invariant amplitude and further of also the cross section of the process, which is obviously in contradiction with the experimental data. The theory is in this state unable to produce any observable (finite) values. An answer for this problem lies in the renormalization. It is worth to mention that so far α_S is true constant with no dependence on any parameter.

The renormalization procedure solves the problem with UV divergences in a way of replacing them to a relations between "bare" quantities and measurable ones¹. For more clear description of the procedure a toy model/theory it is considered with only one free parameter g_0 and a physical quantity $F(x)$ which can be expressed as a perturbative series of this parameter:

$$F(x; g_0) = g_0 + g_0^2 F_1(x) + g_0^3 F_2(x) + \dots, \quad (2.10)$$

$F_n(x)$ are only functions of x . For the purpose it is assumed that one these functions $F_1(x)$ is logarithmically divergent and therefore its form could be defined as follows:

$$F_1(x) = C \int_0^\infty \frac{dt}{t+x}, \quad (2.11)$$

¹"Bare" quantities are represented with a lower index 0 and physical ones without.

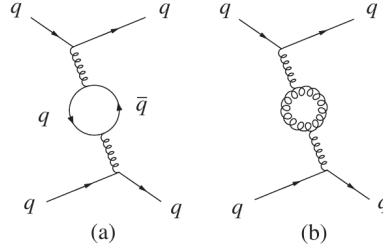


Figure 2.3: The Feynman diagrams of the scattering of quark-quark with the gluon (b) loop and fermion loop (a).[4]

where C is an arbitrary constant. As a real example, could be used QED or QCD with the parameters coupling α_{S0} or electric charge e_0 as the parameter g_0 and the function could represent a cross section of a quark-quark or electron-electron scattering. As was mentioned before and is clear from Equation 2.10, the divergence is included with the higher term proportional to g_0^2 . The method itself is divided into two steps: the *regularisation* and the *renormalization*. The divergences are during the regularization removed and the observable becomes dependent on a auxiliary regularization parameter Λ : $F(x; g_0) \rightarrow F(x; g_0, \Lambda)$. In this simple case, the regularization process is only a cut-off of edges of a divergent integral (the infinity in F_1 is replaced with Λ) but there are many other schemes how can be the regularization done.

Now, the physical observable F should be expressed in the perturbative series of the measurable quantity g :

$$F(\mu) = g, \quad (2.12)$$

where μ is an arbitrary point in which F has been measured (F only depend on g_0 and with this measurement the theory is fully specified) and it is usually called the renormalization scale. For the next progress, the relation between g and g_0 is established and used for the formulation of F in g series (with dependence on μ too):

$$\begin{aligned} F(x; g_0, \Lambda) &= g_0 + g_0^2 F_1(x, \Lambda) + g_0^3 F_2(x, \Lambda) + \dots, \\ g_0 &= g + \delta_1 + \delta_2 + \dots, \end{aligned} \quad (2.13)$$

δ_n are called contrapart terms ($\delta_n \approx g^n$). Last step is removing the parameter Λ with a limit $\Lambda \rightarrow \infty$. If it is the case that the theory is renormalizable

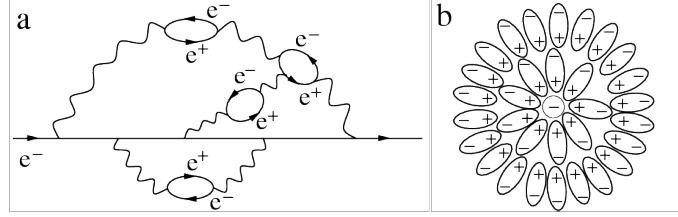


Figure 2.4: The Feynman diagram of a propagation of a electron with the loops (a), the polarization effect of a medium with electric charge (b).[5]

according to renormalizability hypothesis then it should be possible to express F as a well defined perturbative series of the physical parameter g and with dependence on the renormalization scale μ (and also the limit with Λ exists). Whole process can be symbolized:

$$F(x; g_0) \rightarrow F(x; g_0, \Lambda) \rightarrow F(x; g, \mu, \Lambda) \rightarrow F(x) = F(x; g, \mu) = \lim_{\Lambda \rightarrow \infty} F(x; g, \mu, \Lambda) \quad (2.14)$$

The renormalization redefines the bare constant α_{S_0} to the physical one α_S (not only the coupling but also the other parts of Lagrangian are affected and physical opposites ones are defined) [28].

The further text is more focused on a property of coupling $\alpha_{S/E}$ for QCD and QED which is called running, as another consequence of the renormalization. This discussion is going to be led in qualitative manner (only a few final formulas are used) for more information see [29].

In the context of QED it can be explained with help of the Figures 2.4 and the effect called vacuum fluctuations. During this process, a two particle state is created from one particle in accordance with the Heisenberg energy-time relation. For QED it means that from one photon an electron-positron pair can be generated and after a certain time they annihilate back to a photon. For the free photon propagator it means that these vacuum fluctuations/loops have to be included into it (usually called a "dressed" propagator) which causes divergences and they are removed with the renormalization procedure. Results of the process are cancellation of the divergences and a running behaviour of the coupling (the electric charge).

For an external observer it appears to be very similar to the polarization effect for molecules in an electric field which is caused by an electric charge. If they surround this electric charge then a screening effect is applied and

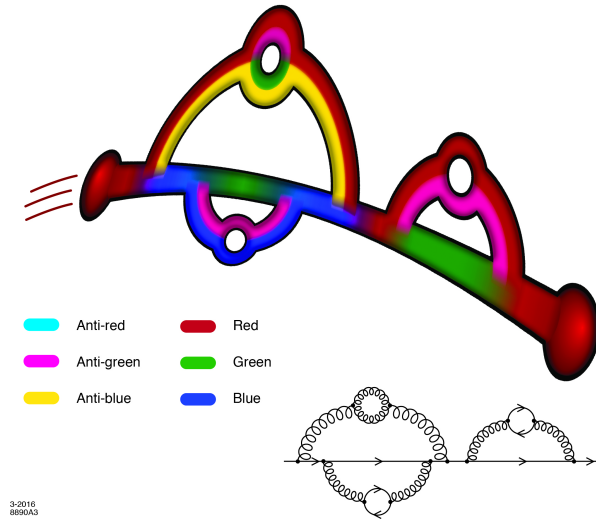


Figure 2.5: The antiscreening effect of QCD with the Feynman diagram of this process. [5]

they decrease its value with the opposite direction of their electric fields to an effective charge, which is lower than the original one. This type of behaviour is due to the abelian nature of QED.

In the previous text it was mentioned that QED, in contrary to QCD, lacks the self interaction of photons. That is the key why in QCD the screening and the opposite effects appear, the anti screening, and for QED only the screening one is included. Almost the same procedure has to be applied for QCD: loops have to be added in the free propagator of a gluon and the renormalization procedure should be used to avoid divergences. Unlike QED, the self interaction of gluons, which in this context means gluon loops (the Figure 2.3 (b)), are also present along the fermion loops (the Figure 2.3 (a)). The overall effect can be seen from Figure 2.5 which shows how the gluon loops increase an effective color charge of a quark, the antiscreening, and how the fermion loops decrease the charge, the screening. In the result the effect of the antiscreening is much more dominant than the screening one and the color charge is increased to the effective one.

Now, the toy model with the observable F is exploited for more quantitative explanation of the running of coupling. A very interesting fact of

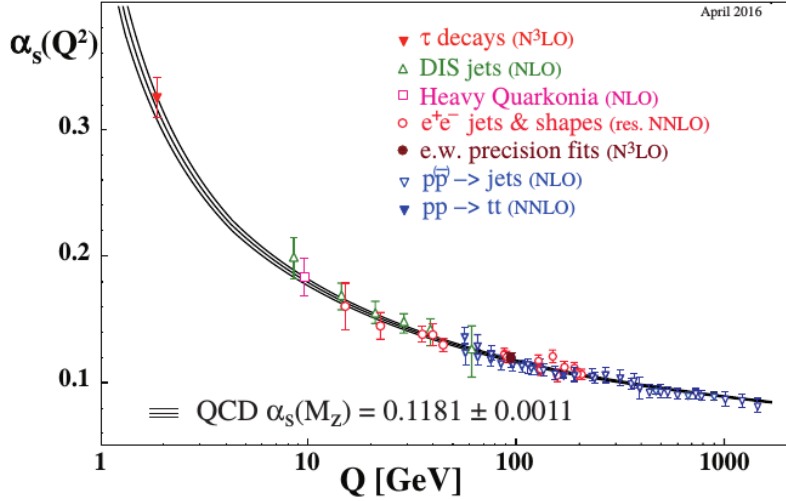


Figure 2.6: The graph of the strong coupling constant α_S as a function of the energy scale Q . [6]

each renormalizable gauge theory is that the precise value of the coupling at some energy scale must be put in the theory; but, on contrary, the dependence on the energy scale is predicted within the theory. In the previous text, the renormalization scale μ was defined as a random point at which the measurement of F had been done and the coupling g acquired a specific value ($g = g(\mu)$). The contingency of the choice of this point means that for another one μ' and a coupling g' a following formula should be valid : $F(x) = F(x; \mu, g) = F(x, \mu', g')$ (still the same prediction for F). It is interpreted as an invariance of the theory when an arbitrary renormalization scale is used. This transformations (in the sense of the pair: (μ, g)) creates a group which is called the renormalization group² and it can be shown that any coupling of this type of theory should meet following equation, renormalization group equation (RGE):

$$mu^2 \frac{d\alpha(\mu)}{d\mu^2} = \beta(\alpha_S(\mu)) = - (b_0\alpha^2 + b_1\alpha^3 + \dots) , \quad (2.15)$$

where $\beta(\mu)$ is the so called beta function and b_0 is the 1-loop coefficient etc.

²This type of group has no dynamical effect or information.

For b_0 in the case of QCD is valid:

$$b_0 = \frac{1}{12\pi}(11C_A - 4n_f T_R) = \frac{1}{12\pi}(33 - 2n_f), \quad (2.16)$$

where $C_A = 3$ is a constant associated with gluon emission from a quark, n_f stands for a number of flavours of quarks and $T_R = \frac{1}{2}$ represents the color factor [6]. If μ is taken close to a momentum transfer of some process ($\mu \approx Q$) than it can be interpreted as relative strength of the strong force. In the perspective of first approximation (the 1-loop coefficient) the RGE can be integrated ($n_f = 3$):

$$\alpha_S(Q^2) = \frac{\alpha_S(Q_0^2)}{1 + \frac{7}{4\pi}\alpha_S(Q_0^2)\ln(\frac{Q^2}{Q_0^2})} = \frac{1}{C\ln(\frac{Q^2}{\Lambda^2})}, \quad (2.17)$$

where $\Lambda \approx 200$ GeV is a constant of divergence of this expression. The running of the coupling is depicted in the Figure 2.6. For a momentum transfer Q going to values near ∞ , the α_S decreases and the strong interaction between them loses its power and quarks behave as free, the asymptotic freedom. At this scale the pQCD is valid and can be used for calculations of strong processes (the scale must be proportional to Λ). On contrary for Q going to values near 0, the α_S increases and the interaction binds quarks in a hadron state, the color confinement. Now, this explains why there is no direct proof which would show the existence of quarks. For this values of Q another approach has to be utilized and most of the time lQCD or another models are exploited.

The further part of the project introduces physical model for a high energy process of hadrons, especially, the hard scattering of protons.

During electron-proton scattering according to the parton model, an electron is interacting with a proton mediated by a virtual photon (corresponds to electro-magnetic interaction), where a distribution of the proton momentum p is reflected with the structure functions $F_1(x, Q^2)$ and $F_2(x, Q^2)$: $Q^2 = -q^2$, q represents a momentum of the photon and $x = \frac{Q^2}{2pq}$ stands for the Bjorken scaling variable³. From the point of view of the parton model, this process is interpreted as an incoherent scattering of a virtual photon on free par-

³It can be expressed as a parton's fraction of the longitudinal momentum of the scattered proton.

tons because the high energy characteristic⁴. This fact allows to define the structure functions as follows:

$$F(x, Q^2) \approx \sum_i x f_i(x), \quad (2.18)$$

where $f_i(x)$ are called the parton distribution function and define a probability that the parton i carries the fraction x of the proton's momentum p (see Figure 2.7). In the frame of this model they are independent of the momentum transfer Q (the Bjorken scaling).

With more discoveries in the field of the strong interaction (for example a gluon) and the resulting improvement of the parton model (at this time, it is not just model but part of QCD) to the quark-parton model, the formula for the cross section of the hadron-hadron (hadron A and B) scattering acquires a following form (consequence of the factorisation theorem):

$$\sigma_{AB} = \sum_{a,b} \int_0^1 dx_1 \int_0^1 dx_2 f_{a/A}(x_1, \mu_F^2) f_{b/B}(x_2, \mu_F^2) \sigma_{ab}(x_1, x_2, \mu_R^2, \mu_F^2), \quad (2.19)$$

where the sum goes over all partons a/b in the hadron A/B , μ_R is the renormalization scale, μ_F is the factorisation scale, σ_{ab} is the cross section between the parton a and b . To modify the formula 2.19 for a practical usage, σ_{ab} should be included in the form of pQCD:

$$\sigma_{ab} = [\sigma_0 + \alpha_S(\mu_r^2)\sigma_1 + \dots]_{ab}, \quad (2.20)$$

where σ_n are members of a perturbative series in the α_S . The combination of this equation and the previous one allows very "simple" approach to the computation of the cross section only with the knowledge of PDFs of protons, which are universal for each process, and the cross sections of partons.

PDF can be divided into two categories: *valence* and *sea* PDF:

$$f_{valence} \equiv f_q - f_{\bar{q}} \wedge f_{sea} \equiv f_{\bar{q}} \quad (2.21)$$

where f_q is PDF of a quark and $f_{\bar{q}}$ is PDF of a antiquark. The definitions represent the fact that in a hadron the creation of a pair quark-antiquark from a gluon is instantly present as also the radiation of a gluon from a

⁴According to the de Broglie wavelength, $\lambda = \frac{\hbar}{p}$, a resolution enlarges with a higher momentum, and the time dilatation, the partons behave as free particle.

quark or a gluon. The consequence of these two processes and already mentioned information are depicted in the Figure 2.7 in a (also in b with some exceptions). It can be seen that the gluon PDF increases (see Equation 2) for very low x and it slowly decreases for higher ones and the same behaviour can be observed for the sea PDF (it is connected with the creation and the annihilation of $q\bar{q}$ to a gluon). A very interesting characteristic of valence PDF is that they can be integrated with almost expected result from the definition of a proton's composition: uud quarks. For this case, a value of the integral of a valence u quark PDF is 2 and of a d quark is 1, which is the wanted result. In this perspective, a more common image of proton as the composite state of two u quark and one d quark and the nowadays approach to a proton with an infinite number of quarks, antiquarks and gluons meet each other.

The reason, why the introduction of factorisation scale in Equation 2.19 was needed, has a relation with new divergences, which occur during a radiation of gluons from partons. This process is governed by the splitting functions $P_{q/g \rightarrow q/g}(x)$ which express the probability that a parton will radiate or split to additional partons with a fraction of his momentum x . For a collinear region (an angle θ between the original parton and the emitted parton goes to 0), the cross section $p \rightarrow p'p^*$ ⁵ can be expressed as follows:

$$\begin{aligned} d\sigma_{p \rightarrow p'p^*} &\approx \frac{\alpha_S}{2\pi} \frac{dy}{y} dx P_{q/g \rightarrow q/g}(x) \approx \frac{\alpha_S}{2\pi} \frac{dp_T^2}{p_T^2} dx P_{q/g \rightarrow q/g}(x), \\ &\rightarrow \frac{\alpha_S}{2\pi} \frac{dp_T^2}{p_T^2} dx \frac{4}{3} \left[\frac{1}{x} + \left(\frac{1}{x} - x \right)^2 \right] \end{aligned} \quad (2.22)$$

where $y = \frac{1+\cos(\theta)}{2}$ is the redefined angle, p_T is the transverse momentum of the emitted parton with the fraction x . To evaluate this equation one is encountered with new infrared (IR) divergences. The first one becomes from the case when a created parton is very near to the initial one ($y \rightarrow 0 \Leftrightarrow p_T \rightarrow 0$), called collinear/parallel divergence, and the second one appears during a radiation of a gluon with zero energy (zero fraction of the momentum), called soft/mass divergence.

The basic principle, on which the cancellation of these divergences depends, is the indistinguishable of a physical state that is a natural preparation for the jets physics. This idea is based on an inclusion of states which

⁵A parton p splits to two partons $p'p^*$.

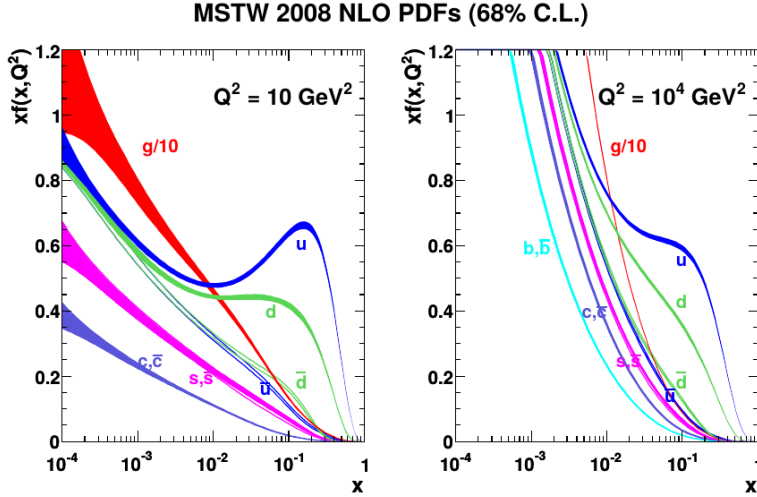


Figure 2.7: The graph of PDF (multiplied by the Bjorken scale x) from the parametrisation MSTW 2008 in the NLO as a function of the Bjorken scale x . [7]

can not be seen (soft/parallel gluon) to the observable ones. It includes some kind of regularisation (cut off) for transverse momentum and energy, which introduces the factorisation scale μ_F and a running characteristic of the parton densities⁶. The factorisation scale is arbitrary and it is usually chosen as a momentum transfer in a process: $\mu_F^2 = Q^2$. For the case of hadron and PDF, μ_R distinguishes between short distance, parton with a higher transverse momentum (see Equation 2) than μ_R , and long distance, soft or parallel parton with a lower transverse momentum than μ_R , behaviour of QCD.

⁶Due to the splitting functions an evolution of PDF as a function of μ_R is not only a differential equation but it is a complex integro-differential equation, called Dokshitzer-Gribov-Lipatov-Altarelli-Parisi equation (DGLAP equation) [30]:

$$\frac{df_i(x, \mu_F)}{\log \mu_F^2} = \frac{\alpha_S}{2\pi} \sum_j \int_x^1 \frac{dx'}{x'} P_{j \rightarrow i}\left(\frac{x}{x'}\right) f_j(x', \mu_F), \quad (2.23)$$

where j goes over all partons that are able to split to parton i and x' is fraction of momentum of the original parton j . Integration is over x to 1 which means that the parton j remains with a new fraction of momentum $\frac{x}{x'}$ after the split. These equations are much more complicated than RGE. Different behaviour/evolution is covered in the Figure 2.7 for values $Q^2 = 10$ and 10^4 GeV^2 .

Chapter 3

Experimental Framework

3.1 LHC and ATLAS detector

The LHC is the most modern and powerful device used for purposes of particle physics. Its main role is to collide accelerated beams of protons or heavy ion nuclei. It is placed in the research centrum CERN in vicinity of the city Geneva at the France-Switzerland border. Nowadays, the highest centre-of-mass energy of the protons beams is $\sqrt{s} = 13$ TeV with a maximum luminosity of $L = 1.58 \times 10^{34} \text{ cm}^{-2}\text{s}^{-1}$. One of the largest experiments, which are installed on LHC, is the ATLAS detector[8] (others included: CMS, ALICE, LHCb).

ATLAS is a multi-purpose detector with an almost 4π coverage in a solid angle. Main parts can be seen in the Figure 3.1. ATLAS is composed of an inner tracking detector (ID), which is surrounded by a superconducting solenoid magnet with a 2 T strength of magnetic field, a middle part electromagnetic and hadronic calorimeters, and the last sub-detector, a muon spectrometer (MS).

The inner tracking detector consists of a pixel detector, a micro-strip semiconductor tracker (SCT) and a transition radiation tracker (TRT). The total range which cover these detectors in pseudorapidity is $|\eta| < 2.5$. Their main purpose is to determine the vertex position and momentum measurement of charged particles with a sufficient precision which is achieved with their high granularity. In May 2014, the ID was upgraded with a new innermost layer of pixel detectors, the Insertable B-Layer (IBL) [31].

The second part of ATLAS, the calorimeters, is divided into inner and

outer level. The inner level consists of the LAr-lead (liquid-Argon) calorimeters with a segmentation to electromagnetic barrel, hadronic and electromagnetic end cap and forward calorimeters. The outer level includes hadronic tile and extended tile barrel from steel and scintillating tiles. The calorimeter gain information about an energy of passing particles through interaction with an absorber (steel, lead) and detection with an active medium (scintillators). The central part (tile barrel) covers pseudorapidity $|\eta| < 1.7$ and the end-cap and forward regions are extended up to $|\eta| < 4.9$. The requirements for the resolution of the calorimeter system is shown in the Table 3.1 (all of them was accomplished with and some of them also overcome).

Detector part	Resolution requirement
EM calorimetry	$\sigma_E/E = 10\%/\sqrt{E} \oplus 0.7\%$
Hadronic calorimetry (jets) barrel and end-cap	$\sigma_E/E = 50\%/\sqrt{E} \oplus 3\%$
forward	$\sigma_E/E = 100\%/\sqrt{E} \oplus 10\%$

Table 3.1: The requirements for the calorimeter system resolution.[8]

The last of the detector is the muon spectrometer which is installed around the calorimeters. Its main task is to determine tracks of muons with very precise system of tracking chambers (region $|\eta| < 2.7$). Indispensable components of the muon spectrometer are three superconducting toroid magnets (one barrel and two end-caps) whose magnetic field perform bending power up to 7.5 T/m (for end-caps and for barrel toroid it is up to 5.5 T/m).

For selection of recorded events from detected ones a trigger system has to be used. It includes two levels where the first one is implemented as a hardware part which reduces the frequency of events to 100 kHz and the second one is a software-based high level trigger with the final output which is less than 1 kHz.

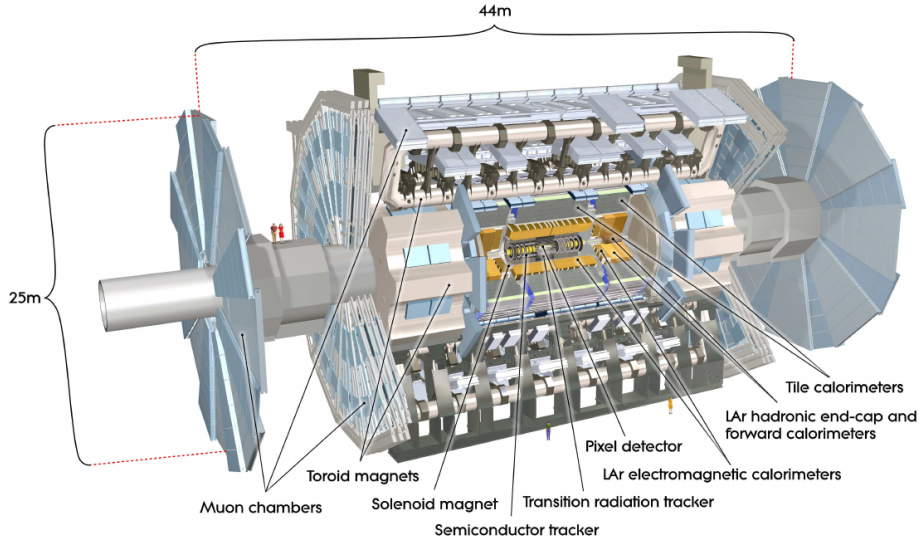


Figure 3.1: The scheme of the detector ATLAS.[8].

3.2 Physics of Jets

This part of the project concerns with the basic principles and definitions of jet physics: ideal properties jet algorithm, jet definition, recombination schemes and a brief characteristic of different types of jet algorithms with most interest in the anti- k_t clustering algorithm (currently the most preferred algorithm in the ATLAS collaboration).

Before the introduction to the jet physics, definitions of the most utilized kinematic variables are needed which is done in the Table 3.2. Only some interesting properties are now discussed: transverse momentum p_T , azimuthal angle Φ and difference of rapidities $y' - y$ are Lorentz invariant, pseudorapidity is a first member of binomial expansion of the logarithm in y and they are equal for the relativistic case. These two values refer to degree of scattering: for $\eta = 0$ a particle is perpendicularly scattered and $\eta = \infty$ a particle continues with the beam's direction.

Jet is a natural and convenient way how to approach problems which are connected with high energy particle processes dominated by the strong force. To summarise (some of these issues), for current detectors there is no possibility to individually measure and record all particles created during their interaction in accelerators and from the theoretical point of view,

Transverse momentum	$p_T = \sqrt{p_x^2 + p_y^2}$
Azimuthal angle	$\Phi = \cotg \frac{p_x}{p_y}$
Rapidity	$y = \frac{1}{2} \ln \frac{p_0 + p_z}{p_0 - p_z}$
Pseudorapidity	$\eta = -\ln \tan \frac{\Theta}{2}$

Table 3.2: The definitions of basic kinematic variable, where the four momentum $p_\mu = (p_0, p_x, p_y, p_z)$, Θ is polar angle between a particle trajectories and z axis of a coordinate system within the center of a detector.

a radiation of a collinear or a soft gluon from a parton is problematic part for computations (emerges IR divergences, see Equation 2). Both of these complications lead to the establishment of a physical object, jet, which includes part of these particles related is some way (near in phase-space or rapidity-azimuthal angular space) and also prevents the occurrence of IR divergences.

Generally, the whole process of collision of two high energy hadrons is a very complicated topic which can not be explained only by pQCD valid for a short-range physics. There are many subprocesses which belong to a domain of soft QCD with respect to energetic scale (they have a long-range behaviour) and phenomenological models are needed for their characterization. To partly understand when and how these distinct processes originate, the hard scattering of protons is further briefly described with the help of Figure 3.2.

During the crossing of accelerated beams in the LHC bunches of protons collide. As mentioned, before the main process of a typical non-elastic collisions is the hard scattering. One of the first experimental problems which has been faced is the *pile-up* effect when more than one hard scatterings of protons happen in the same bunch crossing. For the description in this work, the pile-up effect is neglected and its consequences are no more further discussed and the next description focuses only on single proton-proton scattering¹. According to Figure 2.7, it can be seen that large part of the fraction of proton's momentum is typically carried by one parton and the hard scattering

¹But, it must be remembered that without the pile-up a real simulation of this process would be incomplete and for the current settings of LHC pointless.

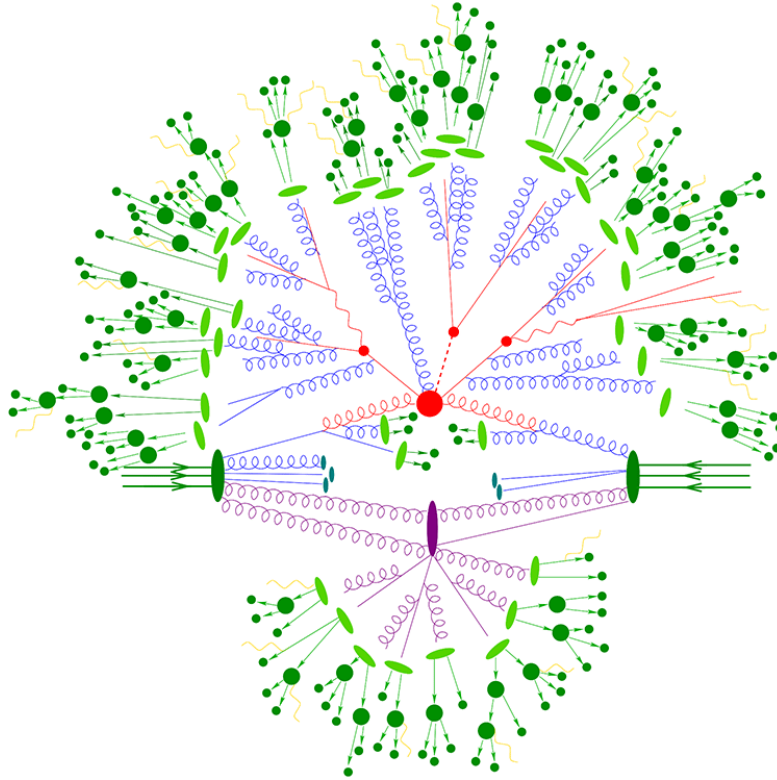


Figure 3.2: The scheme of the hard scattering of two partons with different stages of the process, which are color distinguished: dark green represents the hadronic states, light green stands for the hadronisation process, blue and purple responds to the parton level and with red the partons incoming to hard scattering are marked (further description in Section 3.2). [9]

than takes place between one such parton from each parton. The first subprocess, which happens before the hard scattering, is the *initial state radiation* (ISR) when partons could radiate additional partons. The final result is a creation of so called *parton showers* which is a composite effect of the parton radiation applied on daughter partons. Very similar subprocess to ISR takes place after the hard scattering, the *final state radiation* (FSR). One of the main differences between these two shower effects is their time-like and space-like nature. Whereas ISR manifests as time-like shower, FSR occurs as space-like shower. The *hard scattering of partons* is depicted as the red big bulb and the partons (gluons) as blue helices outgoing from the green incoming protons (the green bulbs with three lines, valence quarks, pointing at them).

Another possibility for interaction is hidden in soft remnants of the protons which are coloured due to the hard scattering of one of the partons. This process is a *multi parton interaction* (MPI) and in Figure 3.2 it is represented as the purple helices, lines and blobs outgoing from the protons. MPI participates in a broader effect called the *Underlying event*, where also pile-up is included.

All these processes are included in the parton level interaction. After this, the hadronization (the bright green) connects coloured objects to hadrons and resonances (the dark green rounds) which can further decay to more stable hadrons (pions). This stage is called the *particle level* and due to the low energy characteristic it has to be described with sQCD, for example Lund string model. The last stage of the process is the *calorimeter level* where the previous particles mostly interact and part of/whole their energy is deposited in the detector[32].

3.3 Jet algorithm

During the development and usage of jet algorithms, many theoretical and experimental requirements have been discovered [10].

- **Fully Specified:** The whole jet algorithm and its aspects should be fully described: selection process, kinematic variables, possible corrections etc.
- **Theoretical well behaviour:** This topic has a close connection to the IR divergences which were mentioned in the Chapter 2 and is illustrated in the Figure 3.3.

The first case of algorithm unwanted sensitivity is a collinear one which is presented in the Figure 3.3 a). So called seed algorithms form a jet around the most energetic particles (seeds). In the left part of the diagram a), the middle particle serves as the seed and the jet is created in its vicinity while in the right part of a), the collinear particle was emitted and therefore the previous seed's energy is decreased which causes that the algorithm finds the new most energetic particle with the following different creation of the jet.

The left part b) of the picture is related to the infrared sensitivity of the algorithm. In the left part of b), the algorithm constructs the two jets around the two particles but in the right part of b), when a radiation of soft particle is present, the algorithm creates the jet around all three particles which is a dangerous behaviour with regard to very high probability of this process.

This behaviour is unwanted and for algorithm is required to not change the content/creation of a jet because of these two effects.

- **Detector Independence:** There should no dependence on the experiment (type of a detector etc).
- **Order Independence:** Jet algorithm should be able to reconstruct jets for each level/order (parton,particle and calorimeter) of a hard process development.

Precise definition of jet is made by the jet algorithm. Generally, they can divided into two basic categories: cone and sequential recombination (cluster)

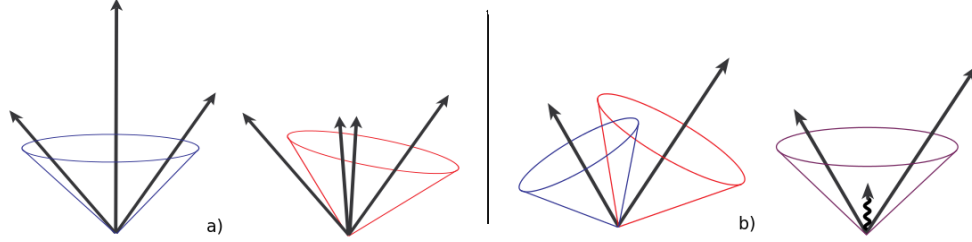


Figure 3.3: The schematic depiction of infrared sensitivity a) and collinear b) of the jet algorithm. Length of the arrow represents the value of energy of a given particle. [10]

algorithms.

Cone algorithm:

Each algorithm, which belong to the class of cone algorithm, can be characterized by an arrangement of particles to a cone. By particles an experimental data from calorimeter (energies) or an other system of a detector (trajectories, momenta) are meant and pseudorapidity azimuthal angle $\eta \times \Phi$ is used as the coordinate system for the cone (if they are massless rapidity instead of pseudorapidity is preferred).

The first step of the jet algorithm with a given dataset is to choose a proper starting particle/value of variable (further all the members of the data are described as objects) and according this feature they can be more distinguished to *seed* and *seedless* algorithms. The difference lies in choice of the most significant object (for example the highest transverse momentum p_T or transverse energy E_T^2) for seed algorithm and for seedless one no kind of this rule is implemented(further only the seed one). The algorithm uses the seed with the characteristics η_K, ϕ_K and absorbs all other objects which are in a cone vicinity defined as:

$$\sqrt{(\eta^i - \eta_K)^2 + (\phi_i - \phi_K)^2} \leq R, \quad (3.1)$$

where R is the radius of the cone. Next step in this process is to determine the kinematic variables of this provisional jet (protojet) which are used in the algorithm. For this purpose the *recombination scheme* is utilized, for

²It can be calculated from the energy E and the polar angle Θ : $E_T = E \sin(\Theta)$

example Snowmass scheme:

$$E_T^K = \sum_{i \in K} E_T^i, \quad \eta^K = \frac{\sum_{i \in K} E_T^i \eta^i}{E_T^K}, \quad \phi^K = \frac{\sum_{i \in K} E_T^i \phi^i}{E_T^K} \quad (3.2)$$

where E_T^i, η^i and ϕ^i is transverse energy, pseudorapidity and azimuthal angle of an i -th object in protojet. There exist many types of recombination schemes and the mostly used is the E-Scheme which defined as only sum of all p_{Ti}/E_{Ti} . With this step, the centre of protojet is shifted and the radius R includes new particles. Therefore, the recombination scheme must be used again and this iterative process continues till the time when there is no change in the position of the centrum of the protojet. Then another seed, which is not comprised in the previous protojet, is chosen and process is repeated. Problem of this algorithm is the possibility of overlapping jets (one or more objects belong to more than one jet). For this reason a *merging procedure* is needed. Another serious issue is the common infrared and collinear sensitivity in the case of a seed algorithm³. This inconvenience was solved in a another type of algorithms, the cluster algorithms.

Cluster algorithm:

The cluster algorithm firstly computes for each pair i, j of objects from a dataset following distances:

$$d_{ij} = \min(k_{Ti}^{2p}, k_{Tj}^{2p}) \frac{\Delta_{ij}^2}{R^2}, \quad d_{iB} = k_{Ti}^{2p} \quad \Delta_{ij} = \sqrt{(y_i - y_j)^2 + (\phi_i - \phi_j)^2} \quad (3.3)$$

where k_{Ti} is momentum of the object i , R is radius in $y \times \phi$ space and p represents a degree of importance of momentum. In the next step the minimum is chosen from these values and if it is d_{ij} then the algorithm unites these two objects i, j into a protojet, with a recombination scheme computes its kinematic variables and returns it to the input dataset. In the case that d_{iB} is the minimum then the object i is labelled as a jet and it is removed from the dataset. The algorithm continues until the input dataset is empty.

³New cone algorithm usually works as seedless and they designed as infrared or collinear safe, for example SIScone algorithm.

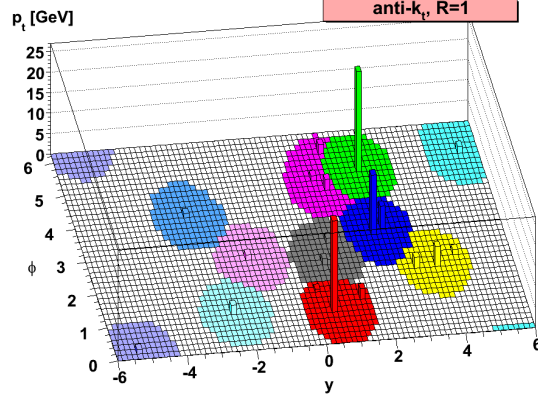


Figure 3.4: The graph of parton level events after usage of anti k_t algorithm.[11]

According to the value of the parameter p , three main types of the cluster algorithms are distinguished: Cambridge-Aachen for $p = 0$, anti- k_t for $p = -1$ and k_t for $p = 1$ algorithm [10].

This type of algorithm, in contrary to others, prefers a creation of jets around particles with the highest momenta. It can be seen from modified Equation 3.3 with the choice $p = -1$:

$$d_{ij} = \min \left(\frac{1}{k_{ti}^2}, \frac{1}{k_{tj}^2} \right) \frac{\Delta_{ij}^2}{R^2}, \quad d_{iB} = \frac{1}{k_{ti}^2}. \quad (3.4)$$

The fractions in the distances d_{ij} and d_{iB} are disproportional to momenta of the objects i, j and therefore the object with higher momentum prioritized which is demonstratively depicted in the Figure 3.4. All jets are constructed around the objects which possesses the highest values of momentum with a regular jet shape of cone determined by the value of the parameter R . The exceptions are present in the case when two high momentum objects are in a distance lower then $2R$. This leads to a distribution of softer objects around the one with higher momentum. Therefore the anti- k_t algorithm manifests a good immunity of the jet shape against a radiation of soft particles [11].

Chapter 4

Monte Carlo prediction of α_S

This chapter focuses on the practical/experimental part of the research project. The main benefit should be the preparation for the measurement of a value of the strong running coupling $\alpha_S(Q^2)$ for some given energetic scale (mostly the mass of Z boson is chosen: $Q^2 = m_Z^2$) in the ATLAS detector at $\sqrt{s} = 13$ TeV. The preparation concentrates on: the general way for determination of the value $\alpha_S(m_Z^2)$, contemporary results for α_S predictions, the Monte Carlo (MC) generator Pythia with a tune and PDF selection including an uncertainty computation, sensible observables for the change of coupling α_S divided to three branches: inclusive and multi jet variables and expected continuation for the diploma thesis.

4.1 Contemporary results for α_S from hadronic final state

The experimental data from high energy collision can be used as a test for pQCD which also includes the prediction of α_S as the running coupling described by RGE. This section summarises current results for the measurement of α_S from the inclusive and the multi jet cross sections (these variables are further discussed and with proper definitions). Several prediction was already performed with a range on the energetic scale Q from 5 GeV to 1400 GeV (range of the α_S values).

One of the first measurements was made at the electron-proton collision with the HERA and the PETRA accelerators in DESY. From this observations (the detectors H1, JADE and ZEUS) the energetic scale from 5 GeV to

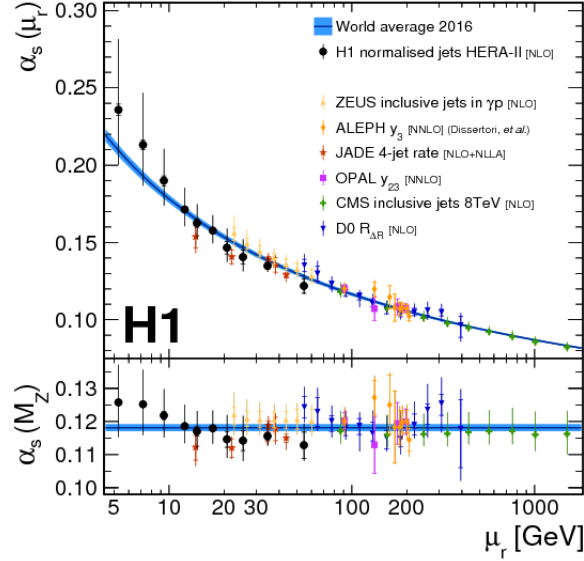


Figure 4.1: The measurement of the α_S with the usage of the colliders: HERA/PERTA, LEP and LHC (CMS). [12]

90 GeV was obtained [33, 12, 34, 35] where the last measurement (see [12]) derived the value: $\alpha_S(m_Z^2) = 0.1172 \pm (0.0004)_{\text{exp}} \pm (0.0053)_{\text{th}}^1$.

The continuation (not chronologically) in the prediction of the α_S value on higher energetic scales from 10 GeV to 210 GeV was made with the CERN accelerator LEP where was produced annihilations of electrons and positrons. For this purposes the detectors ALEPH and OPAL was utilized [36, 37] with the last result from article [36]:

$$\alpha_S(m_Z^2) = 0.1224 \pm (0.0009)_{\text{epx}} \pm (0.0009)_{\text{stat}} \pm (0.0035)_{\text{th}}.$$

Higher energy scale was acquired with the Tevatron collider. For the Tevatron at Fermilab proton-antiproton collisions it was from 50 GeV to 400 GeV with the detector DZero [38, 39]: $\alpha_S(m_Z^2) = 0.1191 \pm (0.0048)_{\text{total}}$. The results for the HERA/PETRA in DESY, LEP in CERN and Tevatron in Fermilab can be seen in the Figure 4.1.

The highest energy measurements were preformed at the LHC for proton-proton collisions with the CMS and ATLAS detectors from 130 GeV to 1400 GeV. For the CMS detector, following center-of-mass energies were

¹The abbreviation "th" is for theoretical and "exp" for experimental uncertainties. Further the abbreviation "tot" is used for total and "stat" for statistical unc.

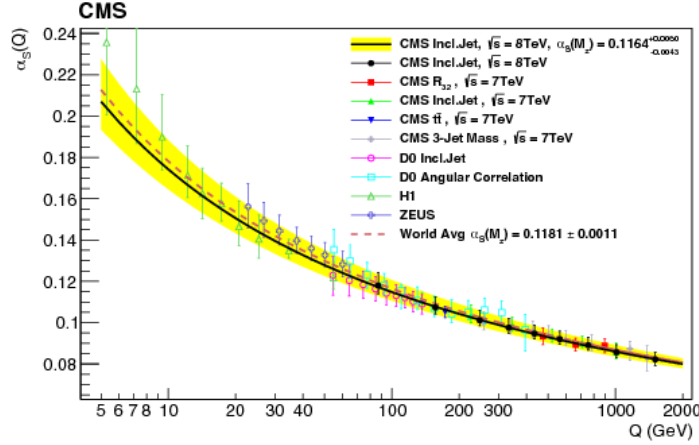


Figure 4.2: The measurement of the α_S with the usage of the detector CMS at LHC. [13]

used: $\sqrt{s} = 2.76$ TeV [13], 7 TeV [40, 41, 42] and 8 TeV [13]. The final result is: $\alpha_S(m_Z^2) = 0.1164^{(+0.0060)}_{(-0.0043)}_{\text{total}}$ and it is shown together with others in the Figure 4.2 (also used variables are included).

The ATLAS detector was exploited with the energy 8 TeV [43, 14] with the final outcome value: $\alpha_S(m_Z^2) = 0.1127^{(+0.0063)}_{(-0.0027)}_{\text{total}}$. The last prediction is depicted in the Figure 4.3.

4.2 Method for α_S prediction

The natural way how extract some information about an object of interests is to measure its properties. General problem occurs when the wanted characteristics can not be measured directly but only as effect/dependency of some different aspect of the object. This example is valid for measuring the value of the strong coupling α_S . For each measurement some variable or a set of variables has to be chosen and they must be expressed as the function of α_S . The exact case was mentioned in the connection with the Equations 2.10 and 2 where these variables are expressed as the perturbative series of α_S . This is the common assumption for the measurement of α_S and can be

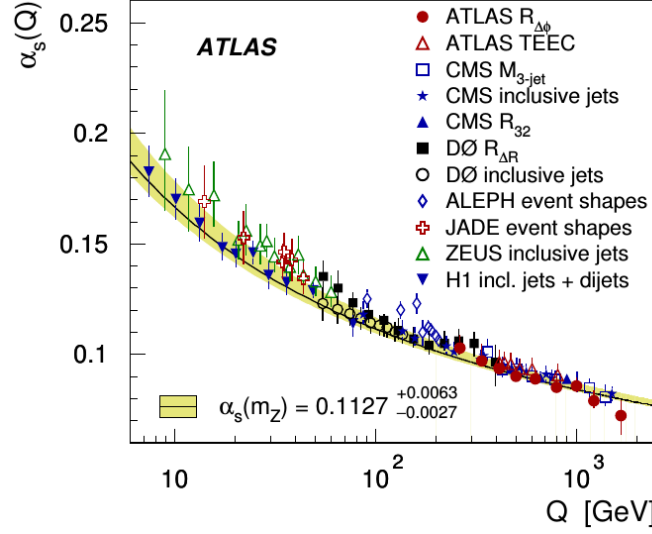


Figure 4.3: The measurement of the α_S with the usage of the detector ATLAS at LHC and also a collection of results from other detectors (and accelerators) is involved. [14]

generally formulated as follows [1]:

$$V_{th}(\alpha_S(\mu_{R/F}), \mu_{R/F}) = \underbrace{\sum_n^N c_n(\mu_{R/F}) \alpha_S^n(\mu_{R/F})}_{\text{pQCD}} + \underbrace{\mathcal{O}(\alpha_S^{N+1}) + \mathcal{O}\left(\frac{\Lambda^p}{Q^p}\right)}_{\text{non-pQCD}}, \quad (4.1)$$

where V_{th} is the theoretical prediction for an experimental variable V_{exp} with the uncertainty δV_{exp} , $c_n(\mu_{R/F})$ are the coefficients of the perturbative series calculated until the order $n = N$, $\mathcal{O}(\alpha_S^{N+1})$ is member which represents the higher orders $N + 1$ and $\mathcal{O}\left(\frac{\Lambda^p}{Q^p}\right)$ reflects a presence of the non-perturbative contributions.

Each member of the Equation 4.1 defines/includes different kinds of possible theoretical uncertainties which together with the experimental result V_{exp} defines total uncertainty of the α_S value prediction:

- δV_{exp} : experimental errors which represents the precision of the observation V_{exp} .
- **pQCD**: comprises the uncertainties from the higher orders $N + 1$ which can not be calculated in the current state of the art.

- **non-pQCD**: effects appear from possible non-perturbative behaviour of the theoretical prediction and it is proportional to the order p of their corrections.

These items constrain the selection of proper variables which should be able to minimize them as much as possible.

4.3 Monte Carlo Generator Pythia

The Monte Carlo generator Pythia 8.235 [44] (further only Pythia 8) has been chosen as a source of input data for this research project. The version 8.235 was used with respect to implemented possibility for computations of PDF uncertainty variations.

Pythia 8 is of the most common MC generators for LHC physics written in the C++ program language ². In the present state, it is capable of simulating collisions between hadrons (protons, pions) and leptons of the same family³ with possible parton and particle data output. One the biggest advantage of Pythia is the opportunity to select a wide range of subprocess with a high variety of other choices (for example: using of MPI with different PDF in contrary to PDF in matrix element computation). Potential inconvenience or disadvantage is the missing implementation of the higher orders of matrix element computation (NLO and further). This fact is balanced/compensated with many models which supply either missing perturbative members of the variable series (replaced with parton showers) or non-perturbative effects (hadronisation). The connection between the LO matrix elements for hard particles/partons and the parton shower for soft and collinear particles could be provided by matching and merging algorithm (for example POWHEG strategy).[45]

4.3.1 Tune and PDF selection

The way how to approach a real data/processes with MC generator is to use the tunes. As was mentioned, Pythia exploits, along the leading order of matrix elements, also phenomenological models or approximations to higher

²Previous most used version Pythia 6 was written in Fortran 77.

³Electron-proton collision is not included.

orders of QCD as parton shower, hadronisation or multiple interaction models to describe effects which far beyond the scope of this first perturbative order of QCD. The problem is that with fully specified models, which were during their compilation in best accordance with an used data, a contradiction during the application in Pythia can occur. For this reason, the models are equipped with a set of free parameters which can be *tuned* for best conformity with current data.

In this work the tune A14 (ATLAS 2014) is used [46] with changed from default settings/tuned MPI, ISR and FSR for leading order PDF: MSTW2008LO[47], NNPDF23LO[48], HERAPDF15LO[49] and CTEQ6L1[50]. During the tuning process a data sensitive to additional jet radiation was utilized: dijet azimuthal decorrelation, the 3/2 ratio etc. In accordance with used A14, the same sets of PDF are used in Pythia.

4.3.2 Theoretical Uncertainty

There are two main sources of the theoretical uncertainties: PDF and the factorization μ_F and renormalization μ_R scale.

For a computation of PDF uncertainties the recommendations of their respective articles/groups or added information in the set itself (see the previous subsection) are followed. The MSTW2008LO and HERAPDF15LO are based on the Hessian method which introduces the set of variations of PDF to some central value. The process uses the χ_{glob}^2 test and its global minimum χ_{min}^2 as the best fit for the N parameters of PDF set⁴. This result is described as the central value F_0 with the set of parameters (a_1^0, \dots, a_N^0) and a new function with a help of the Taylor series is defined (with an assumption that χ_{glob}^2 is quadratic about the minimum):

$$\Delta\chi_{glob}^2 = \chi_{glob}^2 - \chi_{min}^2 = \sum_{i,k=1}^N H_{ik}(a_i - a_i^0)(a_k - a_k^0), \quad H_{ik} = \frac{1}{2} \frac{\partial^2 \chi_{glob}^2}{\partial a_k \partial a_i} \quad (4.2)$$

where H_{ik} is the Hessian matrix which can be further inverted and diagonalized. The result is a group of eigenvalues λ_k and \vec{v}_k eigenvectors ($k \in \hat{N}$). It can be shown that a deviation from the global minimum parameters

⁴Each PDF parametrization is described as a function with some set of parameters which have to be experimentally determined.

(a_1^0, \dots, a_N^0) can be expressed with the usage of these eigenvectors and therefore the parameters variations are defined with some additional condition for the maximal deviation value (and also PDF variations F_k).

Final computation of the theoretical uncertainties for an asymmetrical variations is made according to following formula, called the master equation:

$$\Delta F^+ = \sqrt{\sum_i^N [\max(F_i^+ - F_0, F_i^- - F_0, 0)]^2}, \quad (4.3)$$

$$\Delta F^- = \sqrt{\sum_i^N [\max(F_0 - F_i^+, F_0 - F_i^-, 0)]^2}, \quad (4.4)$$

where $F_i^{+/-}$ are positive or negative variations. For the case of symmetrical variations, the simplified formula can be used:

$$\Delta F^- = \frac{1}{2} \sqrt{\sum_i^N [F_i^+ - F_i^-]^2}. \quad (4.5)$$

Exception is made for the PDF set CTEQ611 where no theoretical uncertainty variations have been done and for NNPDF23LO a different method was utilized (see more discussion in the Source [51]). In this PDF set, the theoretical uncertainties is computed as an "envelope" of the variations to the central value (maximum value from all variations).

A calculation of the scale uncertainties is very similar as is used for the PDF set NNPDF23LO. It is also computed as an "envelope" of variations from default setted values where the following combinations of numbers are used as the multiplicative factors for $(\mu_F; \mu_R)$: (1/2;1), (1;1/2), (1/2;1/2), (2;1), (1;2), (2;2).

The PDF uncertainties is the most dominant from these two a therefore for further discussion only this type is used and computed.

4.4 Data processing and selection of variables

The data were generated from Pythia with the center of mass $\sqrt{s} = 13$ TeV in 17 \hat{p}_T bins from 50 to 4941 GeV (see Table 4.1) with 100 000 events per \hat{p}_T bin as a result from collision of two protons with following set processes:

MPI, ISF, FSR and hard QCD⁵ (and more others from the default and the tune settings). As was mentioned, the anti- k_t jet algorithm was used with the parameter $R = 0.4$ on the particle level. The recombination scheme was chosen as the E-scheme. Both of the are implemented in the interface of the program FastJet (version 3.1.3) [52].

50	200	300	400	500	642	786	894	952
1076	1162	1310	1530	1992	2500	3137	3937	4941

Table 4.1: The edges of \hat{p}_T bins in GeV used for the data generation in Pythia.

For further data processing some cuts had to be applied. The transverse momentum cut $p_{Tmin} = 50$ GeV/c reflects the fact that the calorimeter system has a finite resolution and therefore every possible momentum can not be measured. The same logic is valid for application of the cut for rapidity $y_{max} = 3$ and for variable $y_{max}^* = 3$ (for dijet events) which is defined as with rapidities y_1, y_2 of the two leading jets: $y^* = |y_1 - y_2|/2$ ⁶. For further analysis a new quantities y_{boost} is useful to define: $y_{boost} = (y_1 + y_2)/2$ and $m_{jj} = m_1 + m_2$ where m_1, m_2 are again the invariant masses of two leading jets. These two rapidity quantities reflect the characteristic of the hadron-hadron center-of-mass frame which is longitudinally boosted in the comparison with the center-of-mass frame of the hard subprocess (see Figure 4.4).

The first step after acquisition of data from Pythia was a research of the inclusive cross section distributions which were compared to already published articles about the inclusive cross sections [16]. The following variables were probed: $\frac{d\sigma}{dp_T}$, $\frac{1}{\sigma} \frac{d\sigma}{d\Phi}$, $\frac{1}{\sigma} \frac{d\sigma}{dy}$, $\frac{d\sigma}{dm_{jj}}$ and $\frac{d\sigma}{dp_T y}$. The cross sections $\frac{d\sigma}{dp_T}$, $\frac{d\sigma}{d\Phi}$, $\frac{d\sigma}{dy}$, $\frac{d\sigma}{dm_{jj}}$ and their ratios for different values of α_S with the PDF set MSTW2008LO can be seen in the Figures 4.54.74.84.6. They were used also as a control of correctly set parameters in Pythia and as can be seen no unusual deviations⁷ are not present.

In the comparison with the Figure 4.10, where the inclusive p_T cross section in the intervals of y is shown, a good conformity with the Figure 4.9 can be found (a discussion about the theoretical uncertainties is further).

⁵In Pythia label: HardQCD:all = on.

⁶It is clear that the conditions for y and y^* are the same.

⁷"Jumps" in the distributions or other ill behaviour.

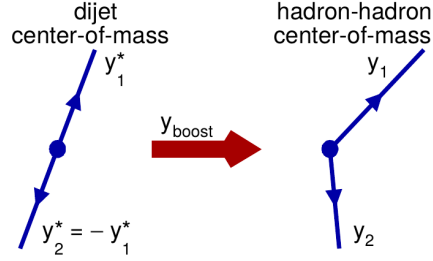


Figure 4.4: The boost effect and the definitions of y_{boost} and y^* . [15]

For the further measurement of the strong coupling α_S value and possible probing of the pQCD theoretical description, variables sensitive to multi jet final states are needed, for example the *multi jet cross sections*. The reason for this type of quantities is due to the proportional behaviour of the higher orders (n -th) of pQCD to $\mathcal{O}(\alpha_S^n)$. For example the dijet event cross section is proportional to α_S^2 and an additional radiation of hard parton in the final state to three dijet event (another vertex has to be included) increases the proportion to α_S^3 .

Few problems are hidden in the usage of the inclusive cross sections. The first one lies in the dependence on a chosen PDF set which is according to Equation 2.23 also dependent on the value of α_S . Therefore the value has to be inserted for the evolution of PDF as a function of $\mu_F = Q$. The second problem occurs with the uncertainty caused by theoretical prediction, precisely, the PDF uncertainties, which have the dominant contribution and blights the effort to perform a precise prediction.

The solution can be found in a normalization procedure when the multi jet variable is divided by an inclusive or a dijet cross section and the uncertainty is reduced. It can be also shown with an experimental data, that the highest experimental uncertainty (the jet energy resolution) is almost cancelled by these ratios. These facts lead to an introduction of ratio multi jet variables as the proper ones for the α_S measurement (for this reasons inclusive cross sections are rejected for further work).

According to this characteristic some quantises with such properties can be constructed. The usually used are following:

- **Dijet Azimuthal Correlation $\Delta\Phi_{dijet}$:** This variable includes the fact about azimuthal distances between two leading jets.

- **Ratio** $R_{3/2}$: The ratio includes information about the ratio of the three jet and the dijet events.
- **Ratio** $R_{\Delta R}$: The ratio comprises the average number of neighbouring jets.
- **Ratio** $R_{\Delta\Phi}$: The ratio contains the variable $\Delta\Phi_{dijet}$ and probe its rapidity and transverse momentum p_T dependence.

In this research project and for further diploma thesis, the dijet azimuthal correlation and probably (in the diploma thesis) the ratio $R_{\Delta\Phi}$ are used as the set of variables. Nevertheless, the option for another choice of variable is still open as well the possibility of complex analysis with usage of more than this set of variables.

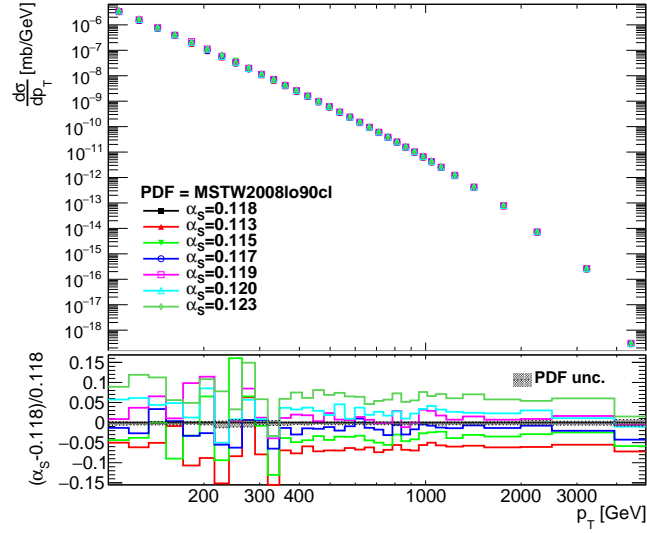


Figure 4.5: The differential inclusive cross section as the function of transverse momentum p_T for different α_S values. The lower graph is the ratio between given α_S and $\alpha_S = 0.118$ normalized to $\alpha_S = 0.118$.

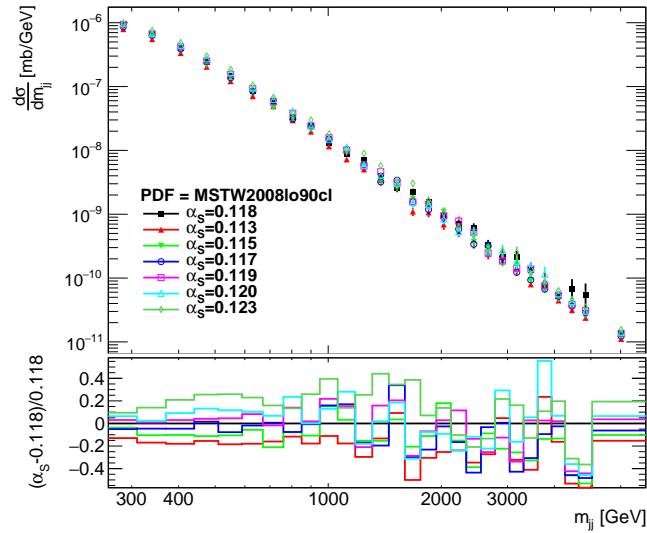


Figure 4.6: The differential dijet cross section as the function of dijet invariant mass m_{jj} for different α_S values. The lower graph is the ratio between given α_S and $\alpha_S = 0.118$ normalized to $\alpha_S = 0.118$.

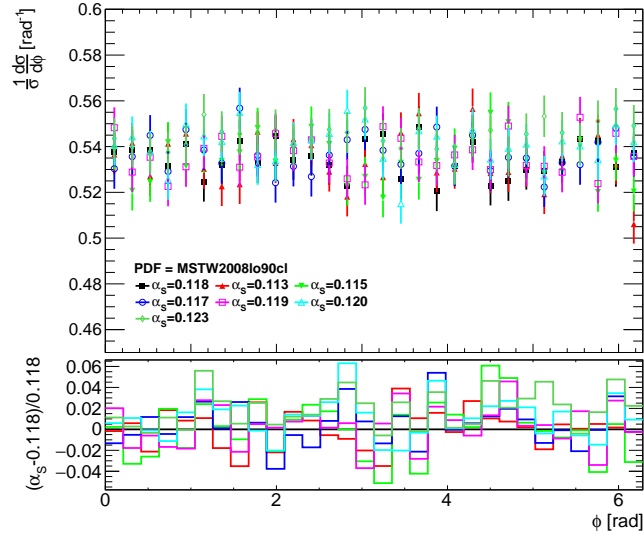


Figure 4.7: The normalized differential inclusive cross section as the function of azimuthal angle Φ for different α_S values. The lower graph is the ratio between given α_S and $\alpha_S = 0.118$ normalized to $\alpha_S = 0.118$.

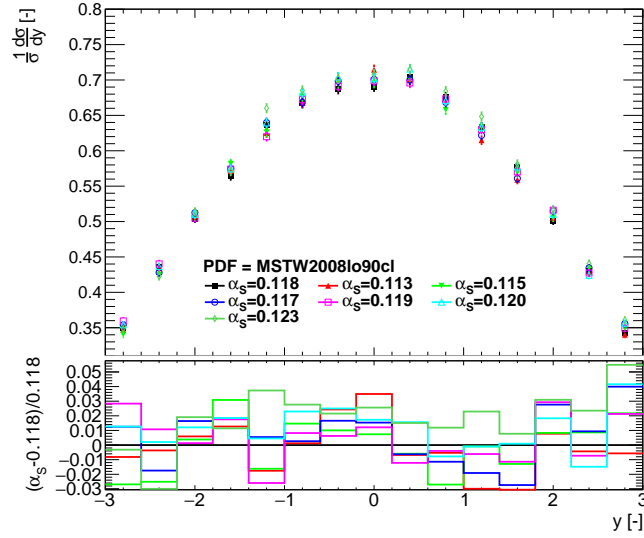


Figure 4.8: The normalized differential inclusive cross section as the function of rapidity y for different α_S values. The lower graph is the ratio between given α_S and $\alpha_S = 0.118$ normalized to $\alpha_S = 0.118$.

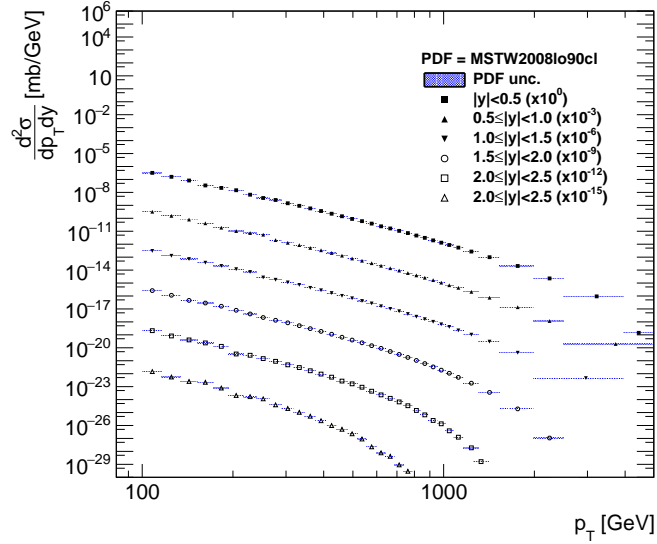


Figure 4.9: The double differential inclusive cross section as the function of transverse momentum p_T in rapidity intervals.

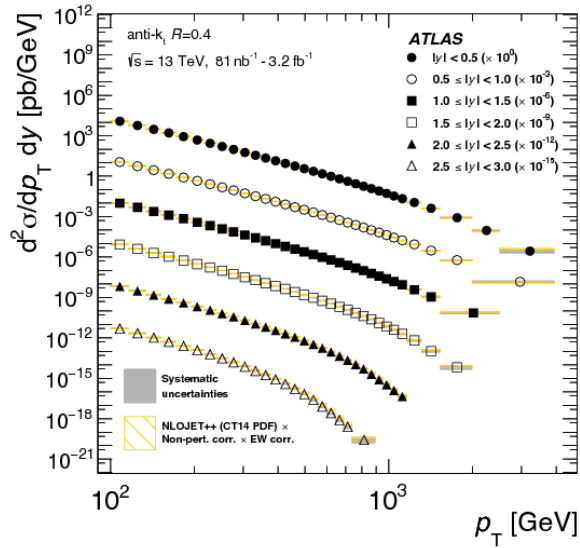


Figure 4.10: The double differential inclusive cross section as the function of transverse momentum p_T and rapidity y . [16]

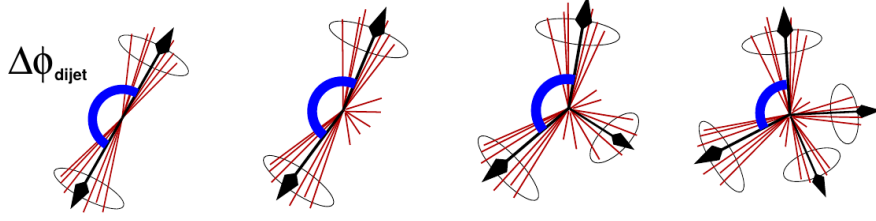


Figure 4.11: The scheme of the azimuthal angle $\Delta\Phi_{dijet}$ for the dijet system with a different number of additional partons. [15].

4.4.1 Dijet Azimuthal Correlation

This quantity includes information about relative azimuthal angle of two leading jets: $\Delta\Phi_{dijet} = |\Phi_1 - \Phi_2|$ (Φ_1, Φ_2 are the azimuthal angles of two leading jets). From the Figure 4.11 can be seen, how precisely is the variable dependent on the additional hard parton radiation in the final state (and on new jet as the further result). In the first situation, when only two leading jets are created, the azimuthal correlation is exactly equal to π which follows from the kinematic constraints. In next schemes, additional parton radiations are produced and this reduces the azimuthal correlation to be less than π . Again, it can be computed from kinematics of this process that the three jet final state is restricted with condition: $\Delta\Phi_{dijet} \geq 2\pi/3$ and the four and multi jet events have to acquire the value: $\Delta\Phi_{dijet} < 2\pi/3$. The way how to approach this variable and use it for the α_S measurement is through the cross section of the event (differential cross section with the dependence on the azimuthal correlation).

From already mentioned facts, the renormalization of $\Delta\Phi_{dijet}$ is necessary. This can be done with the total inclusive dijet cross section σ_{dijet} and the complete definition is following:

$$\frac{1}{\sigma_{dijet}} \frac{d\sigma_{dijet}}{d\Delta\Phi_{dijet}}. \quad (4.6)$$

This observable was already several times measured by the DZero detector at the Tevatron with $\sqrt{s} = 1.96$ TeV [53, 54] and also by the CMS detector at LHC: $\sqrt{s} = 7$ TeV [55], 8 TeV [56], 13 TeV [17] and the ATLAS at LHC: $\sqrt{s} = 7$ TeV [18] (at higher energies a different variable was chosen, see further discussion). The most recent two results for $\Delta\Phi_{dijet}$ are shown in the Figure 4.12.

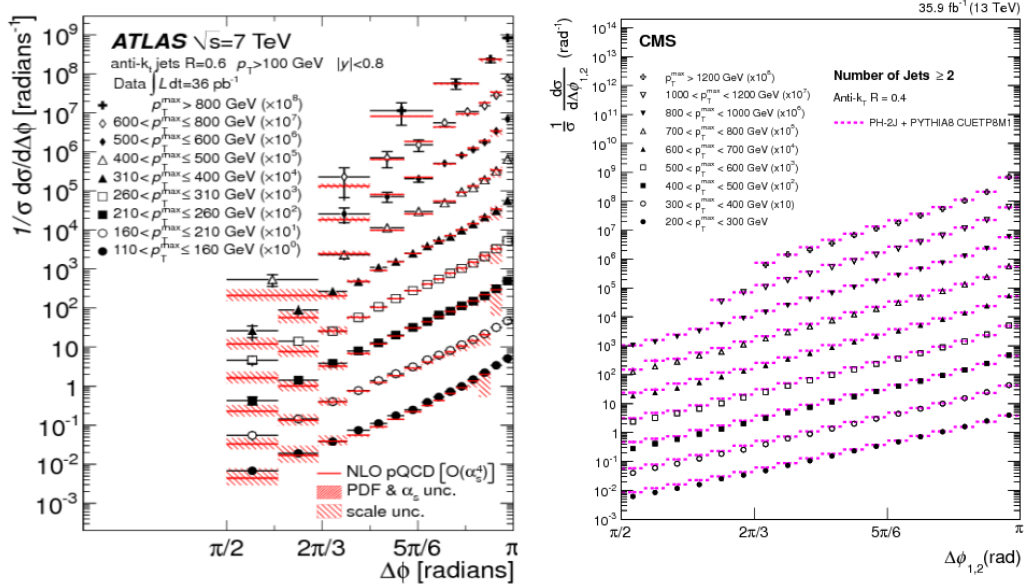


Figure 4.12: The dijet azimuthal correlation by the ATLAS (left) and CMS (right) detector in the p_T intervals [17, 18]

The plot of the $\Delta\Phi_{dijet}$ can be seen in the Figure 4.13. It is shown together with the ratio for different values of α_S and also with the relative theoretical uncertainties caused by PDF for the value $\alpha_S = 0.118$. The very low value of the PDF relative uncertainties can be observed from the Figure 4.14. The disturbing effect is mainly caused by the scales unc. and they restricts which data are used for the α_S value determination. In the frame of this work, same calculation was attempted but with questionable results which indicated very correctly low PDF unc. for the dijet azimuthal correlation but also for the inclusive cross sections. This is with a contradiction with the result from the ATLAS detector [16]. The possible cause is still missing and it should be solved in the diploma thesis.

4.4.2 Ratio $R_{\Delta\Phi}$

The main advantage of this composite quantity is the possibility to express the dependence of the dijet azimuthal correlation $\Delta\Phi_{dijet}$ on transverse momentum p_T and rapidity y and as follows also the same for the pQCD calculations in contrary to $\Delta\Phi_{dijet}$ which is proposed to be only p_T dependent

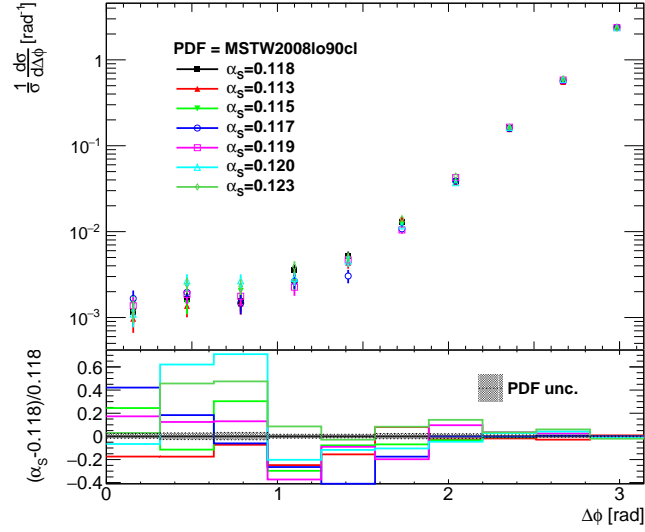


Figure 4.13: The differential dijet cross section as the function of dijet azimuthal correlation $\Delta\Phi$ for different α_S values. The lower graph is the ratio between given α_S and $\alpha_S = 0.118$ normalized to $\alpha_S = 0.118$.

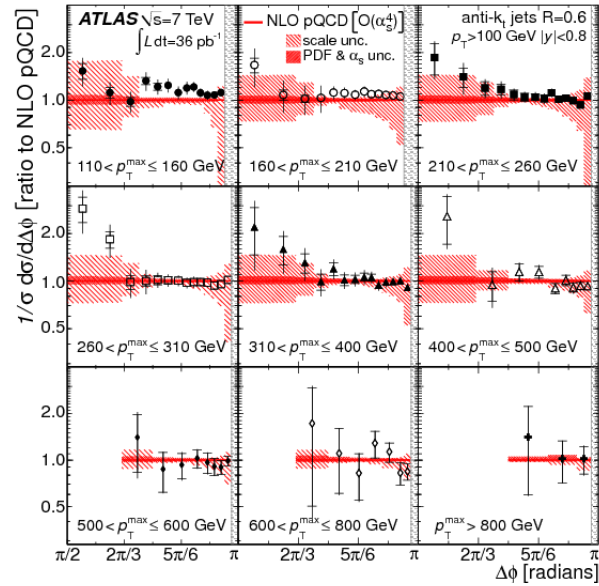


Figure 4.14: The ratio of data and theoretical prediction with the PDF and scale uncertainties.[18]

(see Figure 4.12).

The definition of the ratio $R_{\Delta\Phi}$ has from as follows:

$$R_{\Delta\Phi}(H_T, y^*, \Delta\Phi_{max}) = \frac{d^2\sigma(\Delta\Phi_{dijet} < \Delta\Phi_{max})}{dH_T dy^*} \bigg/ \frac{d^2\sigma(inclusive)}{dH_T dy^*}, \quad (4.7)$$

where the numerator is the double differential cross section of the dijet event which satisfies the condition $\Delta\Phi_{dijet} < \Delta\Phi_{max}$ in variables H_T (it further discussed) and y^* and the denominator is the same double differential cross section but inclusive one. Results for this quantity is expressed in the $\Delta\Phi_{max}$ which corresponds to the topology of the originated final state, the hardness of the two leading jet. This parameter is usually set to be: $7\pi/8$, $5\pi/6$, $3\pi/4$ and $2\pi/3$. The introduction of $R_{\Delta\Phi}$ requires a new momentum variable H_T . The reason lays in the hard multi parton state as the result from the two parton state with the branching process/radiation. The problem why it can not be expressed only as differential of the $P_T = p_{T1} + p_{T2}$ or leading p_T is their noninvariance during the branching process. If more then two jets are created the variable $P_T = p_{T1} + p_{T2}$ and p_T change their values and therefore also the definition for the $R_{\Delta\Phi}$ which could be binned in these variables. Due to this fact, almost invariant H_T is used as scalar sum p_T with the additional conditions:

$$H_T = \sum_{j \in C} p_{Ti}, \quad C = [j | (p_{Tj} > p_{Tmin}) \vee (|y_j - y_{boost}| < y^*)] \quad (4.8)$$

The last result for the center-of-mass energy is shown in the Figure 4.16 for the three regions of y^* : 0.0–0.5, 0.5–1.0 and 1.0–2.0. and can be compared with the picture from the ATLAS detector 4.15 [14]. The main differences between them are mainly caused by distinct binning and by insufficient size of used data sample in Figure 4.15 which causes that some bins disturbs a natural "continues" behaviour (but it is still conserved in the range of the error bars). It is easily to observe how this variable reflects the perturbative QCD topology (LO, NLO) with the different sampling in $\Delta\Phi$.

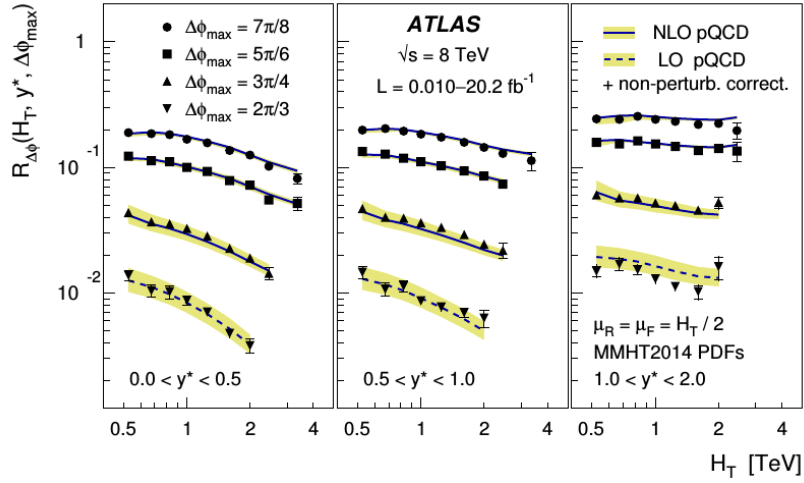


Figure 4.15: The ratio quantity $R_{\Delta\Phi}$ for the different intervals of variables y^* and $\Delta\Phi_{max}$. [14]

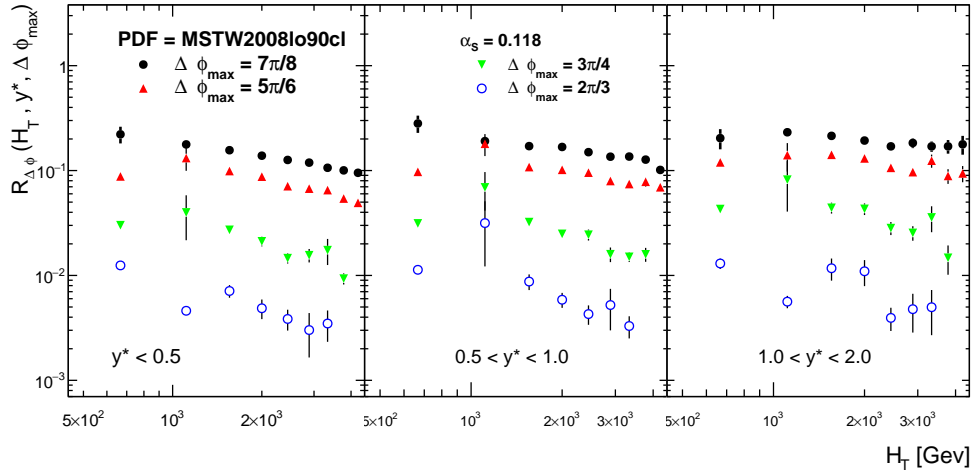


Figure 4.16: The ratio quantity $R_{\Delta\Phi}$ for the different intervals of variables y^* and $\Delta\Phi_{max}$.

4.5 Expected continuation

In the following diploma thesis, many ways for an improvement and continuations are open. The first one is to finish the whole analysis and the measurement with the dijet azimuthal correlation and use it for a quantitative comparison between the theoretical prediction made with Pythia and the experimental data from the ATLAS detector. This procedure itself includes wide range of further subtasks which has to be done, for example: the treatment of experimental uncertainties, unfolding procedure for experimental data, corrections for non-perturbative effects choose some analytical/statistical method to extract the value for α_S .

The second and very probable choice is to generate new data sample for the theoretical prediction with another Monte Carlo generator. In this case, some other generators are for this process available: Herwig or Sherpa (and a few others). This has been already done by my college Vladimír Žitka and it will be further implemented after proper discussion.

Another way could be use some other program for the theoretical prediction than the Monte Carlo generators. For this purposes, the program FASTNLO++ can be exploited. In the current papers, it is a usual manner how the prediction is solved with some advantages in contrary to Pythia., for example fast and easy change of PDF set. This switch between two PDF sets in Pythia and generations with their variations is very time consuming.

Chapter 5

Summary and Conclusion

The purpose of this research project was to become acquainted with topic of the running coupling constant α_S in a theoretical and experimental way and to make a preparation for the following diploma thesis which would focus on the measurement of α_S .

The coupling constant α_S is one of the basic parameters of the Standard Model and participates in almost each calculations of QCD. For this reason the beginning of this work concerns with the theoretical description of the α_S properties in the framework of QCD. The first Chapter 1 aims to introduce the Standard Model as a theory which try to explain the Particle Physics. Further section is dedicated to the historical view of the QCD: from the first attempts to explain hadrons till the proposal of the color charge and the establishment of QCD as the gauge quantum field theory.

The second Chapter 2 discusses the main effects which are related to the coupling constant α_S and to the hard hadron-hadron scattering: the running nature of α_S and the renormalization procedure, quark-parton model and parton distribution functions. It is shown that due to the renormalization of QCD the strong coupling constant becomes running, dependent on the renormalization scale $\mu_R = Q$.

The third Chapter 3 includes basic information about the ATLAS detector and its components, the hard scattering of protons and participated subprocesses like the multi parton interaction, the final state and the initial state showering. The last part is dedicated to jet and jet algorithms and their properties with a further focus on the anti- k_t algorithm.

The last Chapter 4 of this research project deals with the topic of the experimental measurement of the coupling constant α_S and its theoretical

prediction. An introduction to following themes is included: the contemporary results for the α_S value from the PETRA and HERA in DESY, Tevatron in Fermilab and LHC in CERN and method for the α_S prediction.

The main part of the Chapter concerns with the theoretical prediction together with the discussion about proper variable which would be sensitive to perturbative QCD and therefore to α_S . For these purposes, the dijet azimuthal correlation was chosen (and probably for the diploma thesis also the ratio $R_{\Delta\Phi}$) according to the Equation 4.6. The data generation was carried out with the help of the Monte Carlo generator Pythia with ATLAS tune A14. The total number of generated event is 1700000 with center-of-mass energy $\sqrt{s} = 13$ TeV for four PDF sets: MSTW2008LO, CTEQ611, NNPDF23LO and HERAPDF15LO. From this sample, the inclusive cross sections were obtained: $\frac{d\sigma}{dp_T}$, $\frac{1}{\sigma} \frac{d\sigma}{d\Phi}$, $\frac{1}{\sigma} \frac{d\sigma}{dy}$ and dijet $\frac{d\sigma}{dm_{jj}}$ (see Figures 4.54.74.84.6). The double differential cross section $\frac{d^2\sigma}{dp_T y}$ was also compared with the same quantity from ATLAS measurement and the good conformity can be found (see Figures 4.10 and 4.9) which served as the fact of the proper functional data generation. The dijet azimuthal correlation $\frac{1}{\sigma} \frac{d\sigma}{d\Phi}$ is depicted in the Figure 4.13 with the PDF set MSTW2008LO and also the variable $R_{\Delta\Phi}$ in the Figure 4.16 with the same set and $\alpha_S = 0.118$. From the decreasing tendency of $\frac{1}{\sigma} \frac{d\sigma}{d\Phi}$ can be derived the strong dependence on the additional parton radiation and further on α_S which is presented in its ratio plot.

One element of the analysis was the computation of the PDF theoretical uncertainties, which were unsuccessful due to unknown reasons and will be solved for the diploma thesis. It can be deduced that due to the previous conformity in results, the data sample should be at least partly correct and also the theoretical uncertainty computation which was already probed in my bachelor thesis with a correct outcome.

In the last part of the Chapter the possible continuation is mentioned. One of the most probable ways could be the comparison between theoretical prediction presented in this work (after certain improvements) and the experimental data from the ATLAS detector. The computation of the α_S value would be following the step in this analysis. An optional approach might be to exploit another variable then the dijet azimuthal correlation, for example, the ratio $R_{\Delta\Phi}$ or another one. Very essential changes are also still open, for example, to use different Monte Carlo generator (Herwig, Sherpa) or completely different method of theoretical prediction (program FASTNLO++).

Bibliography

- [1] G. P. Salam. The strong coupling: a theoretical perspective. 2017. [arXiv:1712.05165](#).
- [2] D. Galbraith. Standard model of the standard model, 2018. URL: <http://davidgalbraith.org/portfolio/ux-standard-model-of-the-standard-model/>.
- [3] H. Fritzsche. The history of qcd, 2012. URL: <http://cerncourier.com/cws/article/cern/50796>.
- [4] B. R. Martin and G. Shaw. *Particle Physics*. Manchester Physics Series. Wiley, 2008.
- [5] A. Deur, S. J. Brodsky, and G. F. de Teramond. The QCD Running Coupling. *Prog. Part. Nucl. Phys.*, 90:1–74, 2016. [arXiv:1604.08082](#), [doi:10.1016/j.pnpnp.2016.04.003](#).
- [6] C. Patrignani et al. Review of particle physics. *Chin. Phys.*, C40(10), 2016. [doi:10.1088/1674-1137/40/10/100001](#).
- [7] A. D. Martin, W. J. Stirling, R. S. Thorne, and G. Watt. Parton distributions for the LHC. *Eur. Phys. J.*, C63:189–285, 2009. [arXiv:0901.0002](#), [doi:10.1140/epjc/s10052-009-1072-5](#).
- [8] ATLAS Collaboration. The atlas experiment at the cern large hadron collider. *Journal of Instrumentation*, 3(08), 2008. URL: <http://stacks.iop.org/1748-0221/3/i=08/a=S08003>.
- [9] S. Hoeche. Slac - theoretical research - simulations, 2018. URL: <https://theory.slac.stanford.edu/our-research/simulations>.

- [10] G. C. Blazey et al. Run II jet physics. In *QCD and weak boson physics in Run II. Proceedings, Batavia, USA, March 4-6, June 3-4, November 4-6, 1999*, pages 47–77, 2000. URL: http://lss.fnal.gov/cgi-bin/find_paper.pl?conf-00-092, arXiv:hep-ex/0005012.
- [11] M. Cacciari, G. P. Salam, and G. Soyez. The anti- k_t jet clustering algorithm. *JHEP*, 04:063, 2008. arXiv:0802.1189, doi:10.1088/1126-6708/2008/04/063.
- [12] H1 collaboration. Determination of the strong coupling constant $\alpha_s(m_Z)$ in next-to-next-to-leading order QCD using H1 jet cross section measurements. *Eur. Phys. J.*, C77(11):791, 2017. arXiv:1709.07251, doi:10.1140/epjc/s10052-017-5314-7.
- [13] CMS collaboration. Measurement and QCD analysis of double-differential inclusive jet cross sections in pp collisions at $\sqrt{s} = 8$ TeV and cross section ratios to 2.76 and 7 TeV. *JHEP*, 03:156, 2017. arXiv:1609.05331, doi:10.1007/JHEP03(2017)156.
- [14] ATLAS collaboration. Measurement of dijet azimuthal decorrelations in pp collisions at $\sqrt{s} = 8$ TeV with the ATLAS detector and determination of the strong coupling. 2018. arXiv:1805.04691.
- [15] M. Wobisch, K. Chakravarthula, R. Dhullipudi, L. Sawyer, and M. Tamsett. A new quantity for studies of dijet azimuthal decorrelations. *JHEP*, 01:172, 2013. arXiv:1211.6773, doi:10.1007/JHEP01(2013)172.
- [16] ATLAS collaboration. Measurement of inclusive jet and dijet cross-sections in proton-proton collisions at $\sqrt{s} = 13$ TeV with the ATLAS detector. *JHEP*, 05:195, 2018. arXiv:1711.02692, doi:10.1007/JHEP05(2018)195.
- [17] CMS collaboration. Azimuthal correlations for inclusive 2-jet, 3-jet, and 4-jet events in pp collisions at $\sqrt{s} = 13$ TeV. *Eur. Phys. J.*, C78(7):566, 2018. arXiv:1712.05471, doi:10.1140/epjc/s10052-018-6033-4.
- [18] ATLAS collaboration. Measurement of Dijet Azimuthal Decorrelations in pp Collisions at $\sqrt{s} = 7$ TeV. *Phys. Rev. Lett.*, 106:172002, 2011. arXiv:1102.2696, doi:10.1103/PhysRevLett.106.172002.

- [19] S. Moch et al. High precision fundamental constants at the TeV scale. 2014. arXiv:1405.4781.
- [20] J. J. Thomson. Xl. cathode rays. *The London, Edinburgh, and Dublin Philosophical Magazine and Journal of Science*, 44(269):293–316, 1897. URL: <https://doi.org/10.1080/14786449708621070>, arXiv:<https://doi.org/10.1080/14786449708621070>, doi: 10.1080/14786449708621070.
- [21] E. Rutherford. Lxxix. the scattering of α and β particles by matter and the structure of the atom. *The London, Edinburgh, and Dublin Philosophical Magazine and Journal of Science*, 21(125):669–688, 1911. URL: <https://doi.org/10.1080/14786440508637080>, arXiv:<https://doi.org/10.1080/14786440508637080>, doi: 10.1080/14786440508637080.
- [22] M. Gell-Mann. The Eightfold Way: A Theory of strong interaction symmetry. 1961.
- [23] M. Gell-Mann. The interpretation of the new particles as displaced charge multiplets. *Nuovo Cim.*, 4(S2):848–866, 1956. doi:10.1007/BF02748000.
- [24] V. E. Barnes et al. Observation of a hyperon with strangeness minus three. *Phys. Rev. Lett.*, 12:204–206, Feb 1964. URL: <https://link.aps.org/doi/10.1103/PhysRevLett.12.204>, doi:10.1103/PhysRevLett.12.204.
- [25] M. Gell-Mann. A Schematic Model of Baryons and Mesons. *Phys. Lett.*, 8:214–215, 1964. doi:10.1016/S0031-9163(64)92001-3.
- [26] J. D. Bjorken. Asymptotic sum rules at infinite momentum. *Phys. Rev.*, 179:1547–1553, Mar 1969. URL: <https://link.aps.org/doi/10.1103/PhysRev.179.1547>, doi:10.1103/PhysRev.179.1547.
- [27] R. P. Feynman. Very high-energy collisions of hadrons. *Phys. Rev. Lett.*, 23:1415–1417, Dec 1969. URL: <https://link.aps.org/doi/10.1103/PhysRevLett.23.1415>, doi:10.1103/PhysRevLett.23.1415.
- [28] B. Delamotte. A Hint of renormalization. *Am. J. Phys.*, 72:170–184, 2004. arXiv:hep-th/0212049, doi:10.1119/1.1624112.

- [29] F. Gross. *Relativistic quantum mechanics and field theory*. Wiley, 1993.
- [30] T. Plehn. LHC Phenomenology for Physics Hunters. In *Proceedings of Theoretical Advanced Study Institute in Elementary Particle Physics on The dawn of the LHC era (TASI 2008): Boulder, USA, June 2-27, 2008*, pages 125–180, 2010. arXiv:0810.2281, doi:10.1142/9789812838360_0003.
- [31] A. La Rosa et al. The ATLAS Insertable B-Layer: from construction to operation. *JINST*, 11(12):C12036, 2016. arXiv:1610.01994, doi:10.1088/1748-0221/11/12/C12036.
- [32] S. D. Ellis, J. Huston, K. Hatakeyama, P. Loch, and M. Tonnesmann. Jets in hadron-hadron collisions. *Prog. Part. Nucl. Phys.*, 60:484–551, 2008. arXiv:0712.2447, doi:10.1016/j.pnpnp.2007.12.002.
- [33] H1 collaboration. Measurement of Jet Production Cross Sections in Deep-inelastic ep Scattering at HERA. *Eur. Phys. J.*, C77(4):215, 2017. arXiv:1611.03421, doi:10.1140/epjc/s10052-017-4717-9.
- [34] ZEUS collaboration. Inclusive-jet photoproduction at HERA and determination of alphas. *Nucl. Phys.*, B864:1–37, 2012. arXiv:1205.6153, doi:10.1016/j.nuclphysb.2012.06.006.
- [35] S. Bethke, S. Kluth, C. Pahl, and J. Schieck. Determination of the Strong Coupling $\alpha(s)$ from hadronic Event Shapes with $\mathcal{O}(\alpha_s^3)$ and resummed QCD predictions using JADE Data. *Eur. Phys. J.*, C64:351–360, 2009. arXiv:0810.1389, doi:10.1140/epjc/s10052-009-1149-1.
- [36] JHEP collaboration. Determination of the strong coupling constant using matched NNLO+NLLA predictions for hadronic event shapes in e^+e^- annihilations. *JHEP*, 08:036, 2009. arXiv:0906.3436, doi:10.1088/1126-6708/2009/08/036.
- [37] OPAL collaboration. Measurement of event shape distributions and moments in $e^-e^+ \rightarrow$ hadrons at 91 GeV - 209 GeV and a determination of $\alpha(s)$. *Eur. Phys. J.*, C40:287–316, 2005. arXiv:hep-ex/0503051, doi:10.1140/epjc/s2005-02120-6.

- [38] DZero collaboration. Determination of the strong coupling constant from the inclusive jet cross section in $p\bar{p}$ collisions at $\sqrt{s} = 1.96$ TeV. *Phys. Rev.*, D80:111107, 2009. [arXiv:0911.2710](#), [doi:10.1103/PhysRevD.80.111107](#).
- [39] DZero collaboration. Measurement of angular correlations of jets at $\sqrt{s} = 1.96$ TeV and determination of the strong coupling at high momentum transfers. *Phys. Lett.*, B718:56–63, 2012. [arXiv:1207.4957](#), [doi:10.1016/j.physletb.2012.10.003](#).
- [40] CMS collaboration. Measurement of the ratio of the inclusive 3-jet cross section to the inclusive 2-jet cross section in pp collisions at $\sqrt{s} = 7$ TeV and first determination of the strong coupling constant in the TeV range. *Eur. Phys. J.*, C73(10):2604, 2013. [arXiv:1304.7498](#), [doi:10.1140/epjc/s10052-013-2604-6](#).
- [41] CMS collaboration. Constraints on parton distribution functions and extraction of the strong coupling constant from the inclusive jet cross section in pp collisions at $\sqrt{s} = 7$ TeV. *Eur. Phys. J.*, C75(6):288, 2015. [arXiv:1410.6765](#), [doi:10.1140/epjc/s10052-015-3499-1](#).
- [42] CMS collaboration. Measurement of the inclusive 3-jet production differential cross section in proton–proton collisions at 7 TeV and determination of the strong coupling constant in the TeV range. *Eur. Phys. J.*, C75(5):186, 2015. [arXiv:1412.1633](#), [doi:10.1140/epjc/s10052-015-3376-y](#).
- [43] ATLAS collaboration. Determination of the strong coupling constant α_s from transverse energy–energy correlations in multijet events at $\sqrt{s} = 8$ TeV using the ATLAS detector. *Eur. Phys. J.*, C77(12):872, 2017. [arXiv:1707.02562](#), [doi:10.1140/epjc/s10052-017-5442-0](#).
- [44] T. Sjöstrand et al. An Introduction to PYTHIA 8.2. *Comput. Phys. Commun.*, 191:159–177, 2015. [arXiv:1410.3012](#), [doi:10.1016/j.cpc.2015.01.024](#).
- [45] A. Buckley et al. General-purpose event generators for LHC physics. *Phys. Rept.*, 504:145–233, 2011. [arXiv:1101.2599](#), [doi:10.1016/j.physrep.2011.03.005](#).

- [46] A. Buckley. ATLAS Pythia 8 tunes to 7 TeV data. In *Proceedings of the Sixth International Workshop on Multiple Partonic Interactions at the Large Hadron Collider*, page 29, Geneva, 2014. CERN, CERN.
- [47] G. Watt and R. S. Thorne. Study of Monte Carlo approach to experimental uncertainty propagation with MSTW 2008 PDFs. *JHEP*, 08:052, 2012. [arXiv:1205.4024](#), [doi:10.1007/JHEP08\(2012\)052](#).
- [48] S. Carrazza, S. Forte, and J. Rojo. Parton Distributions and Event Generators. In *Proceedings, 43rd International Symposium on Multiparticle Dynamics (ISMD 13)*, pages 89–96, 2013. [arXiv:1311.5887](#).
- [49] A. M. Cooper-Sarkar. HERAPDF1.5LO PDF Set with Experimental Uncertainties. *PoS*, DIS2014:032, 2014. [doi:10.22323/1.203.0032](#).
- [50] J. Pumplin, D. R. Stump, J. Huston, H. L. Lai, Pavel M. Nadolsky, and W. K. Tung. New generation of parton distributions with uncertainties from global QCD analysis. *JHEP*, 07:012, 2002. [arXiv:hep-ph/0201195](#), [doi:10.1088/1126-6708/2002/07/012](#).
- [51] NNPDF collaboration. Parton distributions for the LHC Run II. *JHEP*, 04:040, 2015. [arXiv:1410.8849](#), [doi:10.1007/JHEP04\(2015\)040](#).
- [52] M. Cacciari, G. P. Salam, and G. Soyez. FastJet User Manual. *Eur. Phys. J.*, C72:1896, 2012. [arXiv:1111.6097](#), [doi:10.1140/epjc/s10052-012-1896-2](#).
- [53] DZero collaboration. Measurement of dijet azimuthal decorrelations at central rapidities in $p\bar{p}$ collisions at $\sqrt{s} = 1.96$ TeV. *Phys. Rev. Lett.*, 94:221801, 2005. [arXiv:hep-ex/0409040](#), [doi:10.1103/PhysRevLett.94.221801](#).
- [54] DZero collaboration. Measurement of the combined rapidity and p_T dependence of dijet azimuthal decorrelations in $p\bar{p}$ collisions at $\sqrt{s} = 1.96$ TeV. *Phys. Lett.*, B721:212–219, 2013. [arXiv:1212.1842](#), [doi:10.1016/j.physletb.2013.03.029](#).
- [55] CMS collaboration. Dijet Azimuthal Decorrelations in pp Collisions at $\sqrt{s} = 7$ TeV. *Phys. Rev. Lett.*, 106:122003, 2011. [arXiv:1101.5029](#), [doi:10.1103/PhysRevLett.106.122003](#).

- [56] CMS collaboration. Measurement of dijet azimuthal decorrelation in pp collisions at $\sqrt{s} = 8$ TeV. *Eur. Phys. J.*, C76(10):536, 2016. arXiv: 1602.04384, doi:10.1140/epjc/s10052-016-4346-8.